Phosphatidylinositol 4,5-bisphosphate Impacts Extracellular Vesicle Shedding from *C. elegans* Ciliated Sensory Neurons

Malek W. Elsayyid[1,2], Alexis E. Semmel[1,2], Krisha D. Parekh[1], Nahin Siara Prova[1], Tao Ke[1], Jessica E. Tanis[1]

[1]Department of Biological Sciences, University of Delaware, Newark, Delaware, 19716

[2]These authors contributed equally

Correspondence:

Jessica E. Tanis
105 The Green
233 Wolf Hall
Newark, DE 19716
jtanis@udel.edu

Short Title: PIP_2 impacts ectosome biogenesis

Keywords: cilia, extracellular vesicle, ectosome, *C. elegans,* PI(4,5)P2, PIP5K1, INPP5E

Abstract

Small secreted extracellular vesicles (EVs) mediate intercellular transport of bioactive macromolecules. How the membrane lipid phosphatidylinositol 4,5-bisphosphate (PI(4,5)P_2), which plays a critical role in many cellular processes, impacts EV biogenesis is unclear. The primary cilium, a sensory organelle protruding from most non-dividing cells, transmits signals by shedding EVs called ectosomes. Here, we altered ciliary PI(4,5)P_2 by manipulating expression of the type I phosphatidylinositol 4-phosphate 5-kinase (PIP5K1) PPK-1 and deletion of the phosphoinositide 5-phosphatase (INPP5E) *inpp-1*, then determined the impact on release of EVs that carried cargos tagged with fluorescent proteins. We discovered that increasing PI(4,5)P_2 differentially affected ectosome shedding from distinct compartments, decreasing biogenesis of an EV subpopulation from the ciliary base, but enhancing budding from the cilium distal tip. Altering PI(4,5)P_2 levels also impacted the abundance and distribution of EV cargos in the cilium, but not the sorting of the protein cargos into distinct subsets of ectosomes. Finally, manipulating PI(4,5)P_2 did not affect cilium length, suggesting that changing PI(4,5)P_2 levels can serve as a mechanism to regulate ectosome biogenesis in response to physiological stimuli without impacting cilium morphology.

Summary Statement

Extracellular vesicles (EVs), released from most, if not all, cell types, share bioactive cargo that cannot readily cross the plasma membrane with recipient cells. EVs play numerous roles in physiological processes as well as the propagation of pathophysiological conditions, including cancer, neurodegenerative, kidney, and cardiovascular diseases. Here, we sought to determine the impact of the membrane lipid phosphatidylinositol (4,5)-bisphosphate (PI(4,5)P_2) on EV biogenesis. We used a genetic approach to manipulate PI(4,5)P_2 levels in the primary cilium, a specialized sensory organelle that serves as a platform for signal transmission by shedding EVs. We discovered that high PI(4,5)P_2 differentially impacts two distinct EV subpopulations, decreasing shedding of ectosomes derived from the ciliary base, but increasing budding from the cilium distal tip. This work defines a new role for PI(4,5)P_2 in the regulation of EV biogenesis and ciliary biology.

Introduction

Non-motile primary cilia, sensory organelles enriched with receptors, ion channels, and effector molecules, provide a platform to detect and transduce external signals critical for development and cell homeostasis (Mill et al., 2023). More than thirty human diseases, termed ciliopathies, result from mutations in genes that encode proteins important for cilium structure or function (Mill et al., 2023). In addition to receiving signals, cilia can also transmit signals through the shedding of bioactive extracellular vesicles (EVs) (Luxmi et al., 2019; Wang et al., 2014; Wood et al., 2013). Cilia-derived EVs are utilized for multiple different purposes, including intercellular communication, transfer of signals between animals, regulation of ciliary signaling, and cell waste disposal (Cao et al., 2015; Luxmi and King, 2022; Luxmi et al., 2019; Nager et al., 2017; Ojeda Naharros and Nachury, 2022; Wang et al., 2014; Wang et al., 2020; Wood et al., 2013). Thus, it is important to understand how EV biogenesis from this specialized organelle is regulated.

Contiguous with the plasma membrane, the periciliary membrane compartment (PCMC) at the ciliary base is separated from the cilium proper by the transition zone (TZ), which acts as a gate to confine proteins and lipids into the different compartments (Jensen et al., 2015; Mill et al., 2023; Park and Leroux, 2022). Distinct phosphoinositides, generated by reversible phosphorylation and dephosphorylation of the inositol head groups, bind specific proteins to spatially regulate ciliary processes and signaling (Balla, 2013; Conduit and Vanhaesebroeck, 2020). Phosphatidylinositol (4,5)-bisphosphate (PI(4,5)P_2) is concentrated in the plasma membrane and ciliary base, while phosphatidylinositol 4-phosphate (PI4P) is found at high levels in the cilium proper (Conduit and Vanhaesebroeck, 2020). This phosphoinositide compartmentalization is established by the action of type I phosphatidylinositol 4-phosphate 5-kinases (PIP5K1s), which generate PI(4,5)P_2 from PI(4)P (Conduit and Vanhaesebroeck, 2020; Loijens and Anderson, 1996; Weinkove et al., 2008), and the phosphoinositide 5-phosphatase INPP5E, which is enriched in the cilium proper and dephosphorylates PI(4,5)P_2 to produce PI(4)P (Chávez et al., 2015; Garcia-Gonzalo et al., 2015; Ukhanov et al., 2022). Loss of INPP5E function is the underlying cause of two ciliopathies, Joubert syndrome and MORM syndrome, as well as ciliopathy phenotypes in mice and zebrafish (Bielas et

al., 2009; Jacoby et al., 2009), demonstrating the significance of phosphoinositide compartmentalization in cilia biology.

Stimulation of quiescent cultured cells with serum results in removal of INPP5E from the primary cilium, leading to accumulation of PI(4,5)P_2 in the cilium proper. The increase in PI(4,5)P_2 causes actin polymerization and excision of the cilium distal tip, a process known as cilia decapitation, which results in loss of the primary cilium and cell cycle re-entry (Phua et al., 2017). This excision is distinct from the ectocytosis of small EVs, termed ectosomes, that bud directly from the periciliary membrane compartment (PCMC) and cilium distal tip (Clupper et al., 2022; Nager et al., 2017; Ojeda Naharros and Nachury, 2022; van Niel et al., 2018; Wang et al., 2014; Wang et al., 2021). Whether biogenesis of ciliary ectosomes is regulated by PI(4,5)P_2 as observed for ciliary decapitation remains unknown.

Shedding of bioactive EVs from sensory neuron cilia can be observed in living *C. elegans* (Clupper et al., 2022; Lobo et al., 2025; Maguire et al., 2015; Razzauti and Laurent, 2021; Wang et al., 2014; Wang et al., 2015; Wang et al., 2021; Wang et al., 2024a). Ectosomes that bud from the cilium distal tip play a role in animal-animal communication and are deposited on the vulva during mating (Wang et al., 2014; Wang et al., 2020), while those shed from the PCMC of the ciliary base are taken up by surrounding glia or released into the environment (Clupper et al., 2022; Razzauti and Laurent, 2021). These two EV subpopulations, each with distinct signaling potentials, are differentially shed into the environment in response to the physiological stimulus of mating partners (Clupper et al., 2022; Wang et al., 2021). Ectocytosis of EVs derived from the cilium tip, but not the ciliary base, relies on redundant kinesin-2 motors required for intraflagellar transport (IFT) (Clupper et al., 2022). Together, this indicates that distinct regulatory mechanisms govern EV shedding from the cilium proper versus the ciliary base in a spatially-dependent manner.

Given the known impacts of PI(4,5)P_2 on protein localization, actin dynamics, endocytosis, exocytosis, and membrane deformation (Katan and Cockcroft, 2020), we reasoned that the ciliary compartmentalization of PI(4,5)P_2 could have functional relevance for ectosome biogenesis. We found that in male-specific ray type B (RnB) EV-

releasing neurons (EVNs), the *C. elegans* type I phosphatidylinositol 4-phosphate 5-kinase PPK-1 localizes to and regulates PI(4,5)P_2 abundance in the ciliary base, while the *C. elegans* phosphoinositide 5-phosphatase INPP-1 localizes to and impacts PI(4,5)P_2 in the cilium proper. Using a genetic approach to manipulate PI(4,5)P_2 abundance in ciliary compartments of worms expressing fluorescently labeled EV cargos, we discovered that high PI(4,5)P_2 increases budding of EVs derived from the cilium tip, but inhibits shedding of an EV subpopulation that comes from the PCMC. This altered EV biogenesis is not accompanied by a change in cilium length, suggesting that increasing PI(4,5)P_2 in the cilium proper can serve as a mechanism to enhance EV ectocytosis from the distal tip without inducing ciliary decapitation.

Results

Ciliary PI(4,5)P_2 is regulated by PPK-1 and INPP-1 in EV-releasing neurons

Like in other organisms, PI(4,5)P_2 has been shown to be depleted in the cilium proper of some *C. elegans* ciliated sensory neurons (DiTirro et al., 2019; Jensen et al., 2015), though the distribution of this phosphoinositide in the sensory cilia of the specialized EV-releasing neurons (EVNs) had not been explored. The cilia of the EVNs, which include the inner labial type 2 (IL2), male-specific ray type B (RnB), hook B (HOB), and cephalic male (CEM) neurons, have microtubules with specific structure and post-translational modifications as well as distinct motor proteins that enable abundant EV shedding from the cilium distal tip (Fig. 1A) (Maguire et al., 2015; O'Hagan et al., 2017; Silva et al., 2017). To determine if these unique EVN cilia exhibit phosphoinositide compartmentalization, we used the *klp-6* promoter (Peden and Barr, 2005) to drive expression of a PI(4,5)P_2 reporter consisting of the pleckstrin homology (PH) domain of phospholipase C delta 1 fused to mNeonGreen (mNG::PLCδ1-PH) in the EVNs (DiTirro et al., 2019; Jensen et al., 2015). We co-expressed this integrated, multicopy mNG::PLCδ1-PH transgene with mScarlet-tagged MKS-2 (MKS-2::mSc), a protein in the Meckel syndrome (MKS) complex that localizes to the TZ (Lange et al., 2021). We found mNG::PLCδ1-PH localized to the distal dendrite and PCMC, which is similar to the ciliary pocket in mammals (Molla-Herman et al., 2010), but was excluded from the cilium proper

of the RnB neurons (Fig. 1B). This demonstrates that the EVN cilia use the same phosphoinositide code as other sensory cilia.

In *C. elegans* the sole PIP5K1, PPK-1, generates PI(4,5)P_2 both *in vitro* and *in vivo* and is strongly expressed in the nervous system (Weinkove et al., 2008). GFP-tagged PPK-1 was shown to have a localization pattern similar to that of GFP::PLCδ1-PH in the AWB sensory neurons, though this reporter was not expressed at endogenous levels or imaged with a TZ marker (DiTirro et al., 2019). To define where PPK-1 is localized in the EVNs, we inserted an N-terminal mNG tag on *ppk-1* (mNG::PPK-1) at the endogenous locus and isolated viable animals. This indicates that mNG::PPK-1 has at least partial function, as complete loss of *ppk-1* results in lethality due to its essential role in embryogenesis (Weinkove et al., 2008). Co-expression of mNG::PPK-1 and MKS-2::mSc showed that PPK-1 was present in the dendrite and ciliary base, with significantly lower abundance in the cilium proper (Fig. 1C; Sup. Fig. S1A). We next examined the localization pattern of INPP-1, the *C. elegans* ortholog of INPP5E, which hydrolyses the 5-phosphate from PI(4,5)P_2. Our images of endogenous INPP-1 tagged with mNG at the C-terminus (INPP-1::mNG), co-expressed with MKS-2::mSc, showed abundant INPP-1 in the cilium proper and TZ, but a significant dip in abundance in the PCMC (Fig. 1D; Sup. Fig. S1B). Together, these data show that both PPK-1 and INPP-1 are expressed in the RnB neurons and that these PI(4,5)P_2 regulatory enzymes localize to distinct ciliary compartments in the EVNs.

We next sought to determine how altering levels of PPK-1 and INPP-1 impacted PI(4,5)P_2 abundance in the ciliary base and cilium proper. Since *ppk-1* deletion mutants arrest as larvae, we instead used a transgene to overexpress PPK-1 in neurons (Weinkove et al., 2008). We found that this caused a significant increase in mNG::PLCδ1-PH fluorescence in the ciliary base, but not in the cilium proper (Fig. 2A-C). Since PI(4,5)P_2 only increased where the mNG::PPK-1 endogenous reporter localized, this suggests that the effect is due to overexpression of the kinase. However, we cannot rule out the possibility that overexpression of PPK-1 also causes ectopic expression as it lacks a tag to study localization. Previously, loss of INPP5E in mammalian cells and loss of *inpp-1* in *C. elegans* AWB neurons was shown to cause significant accumulation of PI(4,5)P_2 in primary cilia. Consistent with this, we observed mNG::PLCδ1-PH in the cilium

proper of *inpp-1* mutant RnB neurons, but not wild-type animals (Fig. 2A-C). This indicates that PPK-1 and INPP-1 both act to partition PI(4,5)P_2 in the EVNs (Fig. 2D).

Altering PI(4,5)P_2 in the ciliary base impacts ectosome shedding from this compartment

Having established that overexpression of PPK-1 causes an increase in PI(4,5)P_2 in the ciliary base (Fig. 3A), we sought to determine the impact on EV shedding from this compartment. The calcium homeostasis modulator ion channel CLHM-1 (Tanis et al., 2013) and TRP polycystin ion channel PKD-2 (Barr and Sternberg, 1999) are EV cargoes that were identified through *in vivo* imaging (Clupper et al., 2022; Wang et al., 2014) as well as in an EV proteomic dataset (Nikonorova et al., 2022). These proteins are found in discrete EV subpopulations, with CLHM-1 packaged into EVs shed from the ciliary base and PKD-2 into EVs predominantly shed from the cilium distal tip (Clupper et al., 2022; Wang et al., 2021). To quantitate EVs released into the environment from male tail EVNs, we use total internal reflection fluorescence (TIRF) microscopy to image animals expressing tdTomato-tagged CLHM-1 (CLHM-1::tdT) and GFP-tagged PKD-2 (PKD-2::GFP) single copy transgenes (Clupper et al., 2022). The *him-5(e1490)* mutation, which causes increased frequency of X chromosome nondisjunction (Hodgkin et al., 1979), is in the genetic background of all strains analyzed to generate male offspring for analysis. Previously, we used lambda spectral imaging followed by linear unmixing to demonstrate that CLHM-1::GFP and PKD-2::GFP signal in EVs released into the environment is bona fide GFP emission and not background (Clupper et al., 2022). Here, we show that fluorescent EV-like signals are not detected in *him-5(e1490)* control animals imaged and analyzed under the same conditions as those expressing PKD-2::GFP and CLHM-1::tdT (Sup. Fig. S3A,B). These EVs are likely ectosomes, as individual EVs appear to bud directly from the plasma membrane (Sup. Fig. S3C,D), multivesicular bodies (MVBs) have not been observed in EVN cilia, and MVB components are not required for shedding (Clupper et al., 2022; Wang et al., 2014; Wang et al., 2024b).

We crossed the neuronal PPK-1 overexpression transgene with the CLHM-1::tdT and PKD-2::GFP single copy transgenes and discovered that overexpression of PPK-1

caused a decrease in shedding of the ciliary base-derived CLHM-1-containing EVs, but had no impact on distal tip-derived PKD-2 EV release (Fig. 3B-E). We next examined the colocalization of the ion channel cargos in EVs and found that the probability of PKD-2::GFP being in a CLHM-1::tdT EV was unchanged by PPK-1 overexpression (Fig. 3F). This suggests that while overall shedding of the CLHM-1-containing ectosomes is reduced, the sorting of cargos into these EVs is not disrupted. We then sought to determine how loss of PPK-1 function affects CLHM-1 EV biogenesis. Null mutations in *ppk-1* cause embryonic lethality (Weinkove et al., 2008) and no viable *ppk-1* mutants have been isolated. However, we discovered that the mNG::PPK-1 endogenous reporter strain exhibited significantly reduced brood size and embryonic viability, suggesting that the addition of mNG to the N-terminus of PPK-1 results in a partial loss of function (Fig. 3G,H). We crossed mNG::PPK-1 with the CLHM-1::tdT transgene and found that this reduced PPK-1 function led to a significant increase in the shedding of CLHM-1-containing EVs (Fig. 3I). This suggests that both an increase and decrease in PPK-1 activity affects the release of base-derived CLHM-1 EVs into the environment.

Overexpression of PPK-1 alters ciliary distribution and abundance of EV cargoes

$PI(4,5)P_2$ can impact the ciliary abundance of receptors due to its roles in endocytosis and trafficking (De Craene et al., 2017; DiTirro et al., 2019; Mukhopadhyay et al., 2010; Posor et al., 2015). To explore whether increased $PI(4,5)P_2$ in the ciliary base had an effect on localization or abundance of the EV cargos in the neurons, we crossed the PPK-1 overexpression transgene with CLHM-1::tdT and MKS-2::mNG, then quantified CLHM-1::tdT fluorescence intensity and volume in the different ciliary compartments (Sup. Fig. S2B). While CLHM-1 was present in the ciliary base of all control RnB neurons analyzed, 34% of the RnBs in the PPK-1 overexpressor lacked any detectable CLHM-1 in this compartment (Fig. 4A-C). Overall, PPK-1 overexpression significantly reduced CLHM-1 abundance in the ciliary base, but had minimal impact on CLHM-1 in the cilium proper (Fig. 4B,C). While low CLHM-1 in the ciliary base could explain the decrease in shedding of ectosomes with this cargo (Fig. 3E), we note that a reduction in CLHM-1 abundance in

the PCMC does not necessarily correlate with a decrease in the number of shed EVs (Clupper et al., 2022).

Internalization of channels via clathrin-mediated endocytosis is dependent on PI(4,5)P_2, after which, receptors are sorted for recycling or endosomal degradation (De Craene et al., 2017; Posor et al., 2015). Therefore, we wanted to determine whether enhanced degradation could explain the reduced CLHM-1 EV shedding and ciliary base abundance in animals overexpressing PPK-1. The HRS- (hepatocyte growth factor regulated tyrosine kinase substrate) STAM (signal transducing adaptor molecule) complex binds to and sorts ubiquitinated membrane proteins on the early endosome to the MVB for lysosomal degradation (Bache et al., 2003; Lloyd et al., 2002; Mizuno et al., 2003; Raiborg et al., 2002). The *C. elegans* STAM ortholog, STAM-1, is expressed in the EVNs and PKD-2::GFP accumulates in early endosomes in the ciliary base and distal dendrite of *stam-1* mutant males, suggesting that STAM-1 sorts PKD-2 for lysosomal degradation (Hu et al., 2007). To determine if STAM-1 also promotes the degradation of CLHM-1, we crossed the *stam-1(ok406)* null allele with CLHM-1::tdT and analyzed ciliary abundance. Loss of *stam-1* did not alter the amount of CLHM-1 in the ciliary base, the overall distribution of CLHM-1 in the RnB neurons, or CLHM-1 EV shedding (Sup. Fig. S5A-D). Interestingly, release of PKD-2::GFP EVs was also unaffected by loss of *stam-1*, suggesting that reduced lysosomal degradation of PKD-2 does not enhance shedding of EVs from the ciliary tip (Sup. Fig. S5E). While the HRS-STAM complex acts on early endosomes to sort certain membrane proteins, including PKD-2, to the MVB for lysosomal degradation, our results suggest that a different mechanism is used to down-regulate ciliary CLHM-1. Additional experimentation will be required to identify specific mutants that disrupt the endocytosis and degradation of CLHM-1.

Although PPK-1 overexpression did not impact PKD-2 ectosome biogenesis, analysis of ciliary PKD-2::GFP in these animals showed that high PI(4,5)P_2 in the PCMC disrupted relative abundance of PKD-2 in the different ciliary compartments (Fig. 4D-F). PI(4,5)P_2-binding Tubby (TUB) and Tubby-like (TULP) proteins link ciliary membrane proteins to the intraflagellar transport (IFT) system to mediate trafficking. Thus, the observed increase in PKD-2::GFP in the TZ and decrease in the PCMC suggests that PPK-1 overexpression could impact on trafficking of PKD-2 to the cilium.

Reduced PPK-1 function does not impact CLHM-1 abundance in the RnB neurons

After evaluating the effect of PPK-1 overexpression on the abundance and distribution of EV cargoes in the RnBs, we considered that the increased CLHM-1 EV shedding observed in the mNG::PPK-1 animals, which have reduced PPK-1 function, could also be associated with altered CLHM-1 ciliary abundance. To test this, we crossed mNG::PPK-1 with CLHM-1::tdT and MKS-2::mNG and quantified CLHM-1::tdT fluorescence. Surprisingly, the intensity and volume of CLHM-1::tdT fluorescence in the ciliary base and cilium proper was not significantly different between the mNG::PPK-1 and control animals (Fig. 4G-I). Further, the relative distribution of CLHM-1::tdT between the cilium proper and ciliary base was not affected by reduced PPK-1 function (Fig. 4G; data not shown). This suggests that rather than simply regulating the abundance and localization of EV cargoes within the neurons from which EVs are shed, PI(4,5)P_2 can more directly inhibit ectocytosis from the ciliary base.

Elevated PI(4,5)P_2 in the cilium proper increases EV shedding from the distal tip

Unlike INPP5E mutant mice, which die soon after birth, *inpp-1* mutant *C. elegans* appear essentially normal, despite accumulation of PI(4,5)P_2 in the cilium proper (Fig. 2A-C; Fig. 5A). We created *inpp-1* null mutants that express the CLHM-1::tdT and PKD-2::GFP single copy transgenes to assess how high PI(4,5)P_2 in the cilium impacts EV release. Loss of *inpp-1* significantly increased the shedding of the tip-derived PKD-2-containing ectosomes from the RnBs (Fig. 5B-E; Sup. Fig. S4C,D). However, the average number of CLHM-1 ectosomes as well as the probability of PKD-2::GFP being present in a CLHM-1::tdT EV was unchanged between the control and *inpp-1* mutant (Fig. 5F,G). We note that the effect of INPP-1 on cilium tip versus base-derived EV shedding was recently confirmed by another group using the tetraspanin TSP-6 EV cargo (Lobo et al., 2025). This suggests that high PI(4,5)P_2 in the cilium proper enhances EV shedding specifically from the distal tip.

Given the impact of INPP-1 on PKD-2 EV shedding, we next examined PKD-2::GFP distribution in RnB neuron cilia at two different timepoints. While there was no difference in PKD-2 ciliary localization in the *inpp-1* mutant right after mounting the animals imaging, forty minutes later, we found that PKD-2 was absent from the cilium proper and distal tip in 28% of the *inpp-1* mutant RnB cilia examined, a significantly higher percentage than observed for wild type (Fig. 6A,B). Analysis of only the cilia that initially contained PKD-2 showed that 20% in the *inpp-1* mutants lost PKD-2 signal entirely by the second timepoint, compared to only 8% in the control (Fig. 6C). This suggests that the increase in EV shedding observed in the *inpp-1* mutant may result from all of the PKD-2::GFP in a subset of RnB cilia being released in EVs. Excluding cilia that lacked PKD-2::GFP, loss of *inpp-1* caused a significant increase in PKD-2::GFP fluorescence intensity, without impacting PKD-2 volume in the cilium proper (Fig. 6D,E). While analyzing these images, we noticed that loss of *inpp-1* also caused a significant backup of PKD-2::GFP in the RnB dendrites (Fig. 6F-H). Together, these results indicate that altered phosphoinositide metabolism in the *inpp-1* mutant affects both the abundance and distribution of PKD-2 in RnB dendrites and cilia.

INPP-1 and INPP-5K have both overlapping and divergent functions

Phylogenetic analysis shows that the INPP-5k phosphoinositide 5-phosphatase is the closest paralog to INPP-1 in *C. elegans* with high similarity between the catalytic domains of these phosphatases (Bae et al., 2009). A mutation in *inpp-5k*, previously known by the gene name *cil-1*, was originally identified in a genetic screen for mutants with PKD-2 localization defects in the EVNs (Bae et al., 2008). In *inpp-5k* mutants, there was an increase in PKD-2::GFP in the dendrites, axons, and cell bodies, while PKD-2 localization in the cilium proper appeared unchanged (Bae et al., 2009). We crossed the *inpp-5k(my15)* early stop mutation with a PKD-2::GFP single copy transgene and MKS-2::mSc TZ marker. Loss of *inpp-5k* caused back-up of PKD-2::GFP signal in 71% of RnB dendrites, compared to only 26% of dendrites in the control (Fig. 7A-C). This confirms the effect of *inpp-5k(my15)* on PKD-2 localization, which had previously been observed with a PKD-2::GFP overexpression transgene.

Since the *inpp-1* mutant and *inpp-5k* mutant both exhibited aberrant PKD-2 localization in the RnB dendrites, we hypothesized that these phosphatases could have redundant function in the regulation of PI(4,5)P_2 level in the cilium proper, ciliary abundance of the EV cargoes, and EV shedding. First, to determine if INPP-5k and INPP-1 exhibit a similar localization pattern, we created a INPP-5k::mNG endogenous reporter. *inpp-5k* is expressed in an operon and previous transgenes utilized to look at INPP-5k localization in the EVNs used the *pkd-2* regulatory sequences (Bae et al., 2009). INPP-5k::mNG retains partial function as animals expressing this endogenous reporter had significantly higher brood size compared to *inpp-5k(my15)* mutants, but significantly reduced fertility compared to wild type (Sup. Fig. S6A,B). We observed distinct localization of INPP-5k::mNG to the ciliary base of R6B (Fig. 7D,E) as well as the PHA, PHB, and PHC ciliated neurons in the male tail (not shown). However, INPP-5k::mNG was not present in the ciliary base of RnBs 1-5 and 7-9, which directly contact and release EVs into the external environment (Fig. 7D,E). Further, INPP-5k::mNG was not observed in the cilium proper of any ciliated neurons (Fig. 7D). Considering that the partial function of the INPP-5k::mNG reporter could impact its localization and that loss of *inpp-5k* does cause a phenotype in the RnB dendrites (Fig. 7A-C), we proceeded to investigate PI(4,5)P_2 in the *inpp-5k(my15)* mutant. Loss of *inpp-5k* resulted in a 14% increase in mNG::PLCδ1-PH intensity in the PCMC, just adjacent to the TZ, but had no effect on fluorescence intensity in the cilium (Fig. 7F). This indicates that INPP-1 and INPP-5k do not function redundantly in the cilium proper to regulate PI(4,5)P_2 levels.

We next sought to determine if the dendritic accumulation of PKD-2::GFP observed in the phosphoinositide 5-phosphatase mutants can impact PKD-2 EV release. We found that loss of *inpp-5k* did not alter PKD-2 EV shedding (Fig. 7G), suggesting that the dendritic backup of PKD-2 does not underlie the increase in EVs observed in the *inpp-1* mutant (Fig. 5D,E). These results also show that the different phosphoinositide 5-phosphatases have divergent functions as INPP-1, but not INPP-5k, regulates EV release. Compared to the control, loss of *inpp-5k* did not change the shedding of CLHM-1 EVs or the distribution of CLHM-1 in RnB dendrites (Fig. 7H,I). Thus, altered phosphoinositide metabolism in the *inpp-5k* mutant only influences dendrite enrichment of PKD-2, but not the CLHM-1 ion channel.

An increase in ciliary PI(4,5)P_2 does not impact EVN cilium length

PI(4,5)P_2 in the cilium proper has been shown to impact cilium length by regulating membrane stability and turnover (Jacoby et al., 2009; Stilling et al., 2022; Ukhanov et al., 2022). Highly elevated PI(4,5)P_2 in the cilium proper results in excision of the cilium distal tip, leading to loss of the cilium in a process known as cilia decapitation (Phua et al., 2017). To determine if altered PI(4,5)P_2 abundance impacts the length of EVN cilia, we used a transgene expressing the KLP-6 kinesin-3 fused to GFP to completely fill out the RnB neurons and labeled the TZ with MKS-2::mSc, then measured cilia in PPK-1 overexpressor, *inpp-1* mutant, and control animals (Sup. Fig. S2C). Changing PI(4,5)P_2 levels did not significantly alter the length or diameter of the cilium proper for three different classes of RnB neurons analyzed, although the highest variability was observed in the *inpp-1* deletion mutant (Fig. 8A-C; Sup. Fig. S7A,B). Further, these cilia retain sensory function, as *inpp-1* mutants do not exhibit any defects in mating behavior (Sup. Table S1). These data show that an increase in PI(4,5)P_2 in the cilium proper does not cause ciliary decapitation or shortening of the EVN cilia.

Discussion

The phosphoinositide PI(4,5)P_2 plays critical roles in protein localization, endocytosis, and membrane deformation (Katan and Cockcroft, 2020). Here, using fluorescently-tagged cargoes to visualize EVs, we show for the first time that PI(4,5)P_2 also impacts shedding of signaling ectosomes. High PI(4,5)P_2 levels differentially impacted two distinct EV subpopulations, decreasing biogenesis of CLHM-1-containing ectosomes derived from the ciliary base, but increasing budding of PKD-2 EVs from the cilium distal tip (Fig. 8D). While reduced CLHM-1 EV shedding was associated with lower abundance of the EV cargo in the ciliary base, a decrease in PPK-1 function enhanced CLHM-1 EV shedding without affecting ciliary CLHM-1 levels, suggesting that PI(4,5)P_2 directly regulates ectosome shedding from this compartment. In contrast, an increase in PI(4,5)P_2 in the cilium proper led to time-dependent loss of PKD-2 from distinct cilia, suggesting that the increase in EV shedding from the distal tip of *inpp-1* mutants is the result of abundant

PKD-2 EV release from a subset of cilia. Overall, increasing PI(4,5)P_2 did not impact cilium length, suggesting that PI(4,5)P_2-dependent modulation of ectosome shedding has the potential to regulate EV-mediated signaling without disrupting cilia structure.

We postulate that actin polymerization, which is stimulated by high PI(4,5)P_2 in primary cilia (Phua et al., 2017) and triggers release of tip-derived ectosomes (Nager et al., 2017), causes the enhanced EV release observed in the *inpp-1* mutant. Interestingly, loss of *inpp-1* caused a significant increase in the number of RnB neurons that started with, but then lost all PKD-2::GFP signal in the cilium proper within the timeframe that we analyze EV release. This suggests that heightened EV shedding from a subset of RnB cilia underlies the increase in the number of EVs released in the *inpp-1* mutant. Even with time-lapse imaging, it is not possible to visualize which specific EVs come from each of the 17 individual EV-releasing cilia that express PKD-2 in the male tail. However, to support the idea that altered EV shedding is due to changes in cilium PKD-2, rather than dendritic backup of this protein in the *inpp-1* mutant, we note that aberrant accumulation of PKD-2 in the dendrites of the *inpp-5k* mutant did not affect EV release. This is consistent with the observation that changes in ectocytosis and protein accumulation within a specific ciliary compartment often, though not always, appear to be associated (Clupper et al., 2022; Lobo et al., 2025; Razzauti and Laurent, 2021; Wang et al., 2021).

Overexpression of PPK-1 decreased CLHM-1 abundance in the ciliary base and EV shedding from this compartment. Whether reduced release of CLHM-1 EVs in the PPK-1 overexpressor is the result of PI(4,5)P_2 directly modulating EV biogenesis or due to the changes in cargo enrichment is unclear. Ciliary membrane proteins are internalized at the ciliary base via endocytosis (Clement et al., 2013; Pedersen et al., 2016), a PI(4,5)P_2-dependent process (De Craene et al., 2017; Posor et al., 2015). CAV-1, the ortholog of Caveolin-1, and DYN-1, the ortholog of Dynamin, both localize to the ciliary base and play important roles in endocytosis (Kaplan et al., 2012; Scheidel et al., 2018). Recently, loss of *cav-1* as well as overexpression of dominant-negative DYN-1(K46A), which reduces endocytosis in the ciliary base, was shown to increase release of ciliary EVs containing the tetraspanin TSP-6 (Lobo et al., 2025). Thus, it is possible that higher PI(4,5)P_2 in the ciliary base of the PPK-1 overexpressor causes an increase in CLHM-1 endocytosis, resulting in a decrease in ectocytosis of EVs carrying this cargo. This can

be resolved in future studies by altering PI(4,5)P_2 in the ciliary base of endocytosis mutants, and then determining the impact on CLHM-1 EV shedding. Nevertheless, our results showing that reduced PPK-1 function increases CLHM-1 EV shedding without affecting ciliary abundance of this cargo indicate that PI(4,5)P_2 can directly inhibit ectosome release from the ciliary base. Since PI(4,5)P_2 has opposing effects on ectocytosis from the base compared to the cilium tip, we hypothesize that PI(4,5)P_2 acts by different mechanisms to regulate EV shedding from the compartments. While the mechanism by which PI(4,5)P_2 inhibits EV release from the ciliary base is completely unresolved, it is intriguing that ARF6 and RhoA, two proteins that promote ectosome biogenesis, both activate PIP5K1, the mammalian ortholog of PPK-1 (Honda et al., 1999; Li et al., 2012; Muralidharan-Chari et al., 2009; Weernink et al., 2004). Given that PPK-1-dependent changes in PI(4,5)P_2 alter the quantity of EVs released, it is possible that ARF6 and RhoA not only mediate EV ectocytosis, but also regulate the overall amount of shedding.

Phosphoinositide metabolism impacts the localization and abundance of ciliary proteins through effects on trafficking between different ciliary and membrane compartments (Bae et al., 2009; DiTirro et al., 2019). Overexpression of PPK-1 in the ciliary base altered the relative distribution of PKD-2, possibly affecting IFT of this protein. Tubby (TUB) and Tubby-like (TULP) proteins rely on PI(4,5)P_2 to link ciliary membrane proteins to the IFT system in the PCMC, while low PI(4,5)P_2 in the cilium proper is thought to weaken this interaction and allow for cargo release (Chávez et al., 2015; DiTirro et al., 2019; Garcia-Gonzalo et al., 2015; Mukhopadhyay et al., 2010; Mukhopadhyay et al., 2013). Phosphoinositides are also required to direct the trafficking of proteins between endocytic compartments (Bae et al., 2009). While loss of *inpp-5k* caused aberrant accumulation of PKD-2 in the ciliary base and RnB dendrites, CLHM-1 localization in the RnBs was unaffected. Previously, the localization of other ciliary proteins including IFT components OSM-6 and BBS-5, the TRPV ion channel OSM-9, and the G-protein coupled receptor ODR-10 was found to be unchanged in the *inpp-5k* mutant. Together, this shows that phosphoinositide metabolism is required for proper distribution and degradation of some, but not all ciliary proteins.

How compartmentalization of phosphoinositides in the cilium is established and maintained is not completely understood. Here we show that PPK-1 and INPP-1 localize to the ciliary base and cilium proper, respectively. Loss of *inpp-1* increased PI(4,5)P_2 in the cilium proper, while PPK-1 overexpression did not, likely due to the intact TZ. Loss of the TZ protein MKS-5 results in abnormal PI(4,5)P_2 accumulation in the cilium proper (Jensen et al., 2015), although whether this is due to mislocalization of PI(4,5)P_2 regulatory enzymes, or because the TZ acts as a lipid diffusion barrier (Park and Leroux, 2022) is unknown. Interestingly, TZ mutants also have defects in EV shedding (Wang et al., 2024a), which could result from loss of PI(4,5)P_2 compartmentalization. Future work assessing both the abundance and localization of PI(4,5)P_2, INPP-1, and PPK-1 in TZ mutants would shed light on the mechanism by which specific TZ proteins contribute to the ciliary compartmentalization of PI(4,5)P_2 to regulate protein enrichment and ectosome release.

Loss of *Inpp5e* or rapid synthesis of PI(4,5)P_2 in the cilium proper has previously been shown to reduce cilia length through a process known as ciliary decapitation (Jacoby et al., 2009; Phua et al., 2017; Stilling et al., 2022). As a result, INPP5E mutations in humans cause cilium instability and signaling defects, resulting in ciliopathy syndromes (Bielas et al., 2009; Jacoby et al., 2009). We found that the increase in cilium PI(4,5)P_2 and tip-derived EV shedding in the *inpp-1* mutant did not change RnB neuron cilium length or morphology. We considered that there could be another redundant phosphatase that prevents PI(4,5)P_2 from reaching a level that would induce ciliary decapitation. Loss of the other *Inpp5e* ortholog in *C. elegans*, *inpp-5k*, did not alter the PI(4,5)P_2 level in the cilium proper or PKD-2 EV release from the distal tip. In contrast, a recent study found that there was increased ciliary EV shedding from the PHA/PHB neurons in the *inpp-5k* mutant (Lobo et al., 2025). This could be because INPP-5k localizes to the ciliary base in the PHA/PHB neurons and R6B, but not in the RnBs that release abundant PKD-2 EVs from the distal tip and into the environment. There are multiple other phosphoinositide 5-phosphatases that can dephosphorylate PI(4,5)P_2, including OCRL, which localizes to primary cilia in other organisms (Conduit et al., 2012; Jacoby et al., 2009; Zhang et al., 1995). Knockdown of OCRL1 in cultured cells and zebrafish causes ciliary defects (Luo et al., 2012; Rbaibi et al., 2012). We tagged *C. elegans* OCRL-1 with mNeonGreen at the

endogenous locus, but did not observe localization to the cilium proper in the EVNs (data not shown). The synaptojanin ortholog UNC-26, which is required for synaptic vesicle endocytosis and recycling, also exhibits sequence similarity with INPP-1, however, *unc-26* mutants do not cause defects in ciliary PKD-2 localization (Bae et al., 2009). Thus, while we cannot rule out the presence of additional phosphoinositide 5-phosphatases in the RnB cilia, we suggest that since these EVNs are terminally differentiated, this increase in PI(4,5)P_2 in the primary cilium may regulate ectosome biogenesis rather than induce ciliary decapitation.

EV shedding can affect protein composition of the cilium and remove activated receptors to control signaling in the releasing cell (Nager et al., 2017), while uptake of EVs can impact signaling in surrounding cells (van Niel et al., 2018) and play a role in inter-organism communication (Wang et al., 2014; Wang et al., 2020). Here we consider how ciliary abundance and compartmentalization of PI(4,5)P_2 could be controlled in living animals to regulate EV release. External stimuli can dynamically regulate protein content in both the cilium proper and EVs (Clupper et al., 2022; DiTirro et al., 2019; Nager et al., 2017; Wang et al., 2021). Interestingly, compromised sensory signaling in the ciliated sensory AWB neurons increases trafficking of PPK-1 into the cilium proper, and thus, PI(4,5)P_2 (DiTirro et al., 2019). This raises the possibility that sensing of mate availability, which impacts EV release (Clupper et al., 2022; Wang et al., 2021), or other mating cues (Srinivasan et al., 2008) by the EVNs, could alter the localization, abundance or activity of the proteins that regulate PI(4,5)P_2 levels. While *inpp-1* mutants have diminished sensory response and olfactory habituation in response to low concentrations of diacetyl (Larsch et al., 2015), we found that loss of *inpp-1* did not affect male mating behavior. Thus, it is conceivable that altering PI(4,5)P_2 in the RnB neurons could change the signaling potential of EV release without affecting male mating competency.

Materials and Methods

C. elegans strains and maintenance

All strains were cultured at 20°C on Nematode Growth Media (NGM) plates seeded with OP50 *E. coli*. *stam-1(ok406)* I, *inpp-5k(my15)* III, *inpp-1(gk3262)* IV and *him-5(e1490)* V

mutant alleles, *ppk-1*(*syb8819 [mNG::ppk-1])* I, *mks-2*(*oq101 [mks-2::mNG]*) II, *mks-2(syb7299 [mks-2::mSc])* II, *inpp-5k(syb9399 [inpp-5k::mNG])* III, and *inpp-1(syb3371 [inpp-1::mNG])* IV endogenous insertion alleles, *gqIs25 [rab-3 promoter::ppk-1]* I, *myIs10 [klp-6 promoter::klp-6::GFP]*, and *henIs1 [klp-6 promoter::mNG::PLCδ1-PH]* V integrated transgenes, and *henSi3 [clhm-1 promoter::clhm-1::tdT]* III, *henSi20 [pkd-2 promoter::pkd-2::GFP]* IV, and *henSi21 [pkd-2 promoter::pkd-2::GFP]* V single copy transgenes were utilized. Duplex genotyping was used to detect *stam-1(ok406)* and *inpp-1(gk3262)*; SuperSelective genotyping was used to detect *inpp-5k(my15)* (Touroutine and Tanis, 2020). The presence of fluorescent transgenes was determined by visual screening. See Supplementary Table S2 for a list of all strains used in this work. Some of these strains are available from the *Caenorhabditis* Genetics Center (CGC); all others are available upon request.

Generation of the PI(4,5)P_2 sensor

The construct used to express the PI(4,5)P_2 sensor mNG::PLCδ1-PH in the EVNs was created using restriction enzymes for cloning. mNG containing synthetic introns, with no stop codon, and followed by the flexible linker GSSGSSGTS was amplified from Addgene plasmid #177338 pGLOW77 (Witten et al., 2023) and inserted into pENM1, a plasmid which contains the 1.58 kb *klp-6* promoter (Clupper et al., 2022). The PH domain of phospholipase C delta 1 (Stauffer et al., 1998) was amplified from Addgene plasmid #21179 (GFP-C1-PLCdelta-PH) and inserted following the flexible linker at the C-terminal end of mNG. This *klp-6* promoter:: mNG::PLCδ1-PH plasmid pJT174 (2 ng/µl), pCFJ421 (*myo-2* promoter::GFP::H2B; 5 ng/µl) (Frøkjær-Jensen et al., 2012), and genomic DNA (90 ng/µl) were injected into wild-type animals using the standard germline transformation technique to generate a complex array (Kelly et al., 1997). We screened five lines and chose to proceed with the strain that had the lowest expression and did not disrupt the morphology of the RnB neurons. Part of the resulting extrachromosomal array was integrated into the *him-5* locus using CRISPR/Cas9 genome editing. Two gRNAs specific for the *him-5* locus and one gRNA to target the pJT174 backbone to fragment the extrachromosomal array were injected along with a *dpy-10* cRNA and *dpy-10* repair

oligonucleotide harboring the dominant *cn64* mutation. In the F1 generation, animals with the dominant Roller phenotype were cloned to enrich for animals with CRISPR/Cas9 edits (Arribere et al., 2014). We screened resulting F2 progeny and selected four plates that appeared to have significantly more animals with GFP in the nuclei of the pharyngeal muscles (pCFJ421) compared to the starting strain with the extrachromosomal array. Eight worms were cloned from each of these plates and the F3 animals were screened for fluorescence. One plate had animals that exhibited 100% fluorescence and a *him* phenotype; this integrated transgene is designated *henIs1.*

RnB neuron and cilia imaging and analysis

Imaging of RnB neurons was performed on adult males 24 hours post fourth larval (L4) stage. *C. elegans* were immobilized with 50 mM levamisole (ThermoFisher Cat #: AC187870100) pipetted onto 3% agarose pads on microscope slides and Z-stack images of splayed male tails were acquired with an Andor Dragonfly microscope (63x objective) and Zyla sCMOS camera. Identical image acquisition settings were used for all images that were directly compared; control and experimental strains were always imaged on the same day. The “multi plot” function in ImageJ (NIH) was used to plot fluorescence intensity distribution of mNG::PLCδ1-PH, mNG::PPK-1, INPP-1::mNG, INPP-5K::mNG, CLHM-1::tdT and PKD-2::GFP along a 6 µm linear ROI that was drawn through the entirety of the cilium and base for R3B-R5B neurons (Sup. Fig. S2A) using a maximum intensity projection. For each measurement, the center of the TZ as determined by MKS-2::mSc fluorescence was positioned at 3 µm. While average TZ length in the representative images shown in all figures was 1.09 +/- 0.06 µm, variability in some images resulted in a spread in MKS-2::mSc signal as observed in Figure 1. In normalized intensity plots, all values were normalized to the maximum intensity value in the line scan ROI. RnBs with aberrant PKD-2 accumulation in the dendrites were defined as those with PKD-2::GFP signal extending greater than 5 µm from the TZ. Binary scoring was used to classify each RnB cilium as either having PKD-2 present (score = 1) or absent (score = 0), if no PKD-2::GFP signal was detected using a threshold of 16 in Imaris.

Imaris (Oxford Instruments) was used for quantitative volumetric and fluorescence intensity analysis of the cilium proper and cilium base in three-dimensional reconstructions (Sup. Fig. S2B). A ROI was drawn around the ciliary region of each RnB analyzed and a constant, preset intensity threshold, which was dependent on the fluorescent protein being analyzed, was used to select the fluorescence signal and create a corresponding surface using the surfaces tool for the cilium proper and ciliary base. Cilia without PKD-2 were defined as those that lacked detectable PKD-2::GFP signal in the cilium proper using the Imaris surfaces tool at a threshold of 16. For ciliary length and diameter analysis, surfaces were first made to encapsulate the TZ. A ROI was then drawn to exclude the TZ surface but enclose the KLP-6::GFP-labeled cilium proper. The filament tool was used to draw the cilium structure in 3D space given a set segment seed point threshold (=160); lengths of each filament were recorded (Sup. Fig. S2C).

EV imaging and analysis

All transgenes used to quantitate EV shedding were integrated into the genome at single copy, since overexpression can impact EV cargo selection and release (Razzauti and Laurent, 2021). Our *C. elegans* strains have been acknowledged as an *in vivo* model in which to analyze EVs in the most recent MISEV position paper (Welsh et al., 2024). Eight transgenic L4 hermaphrodites carrying the *him-5(e1490)* mutation and single copy transgenes expressing fluorescent protein-tagged EV cargos were picked onto 6 cm NGM plates and allowed to grow for 4 days, resulting in a mixed population of adult males and hermaphrodites. Adult males were picked from an unseeded region of the NGM plate to prevent contamination from the *E. coli* food source, then picked into 20 mM levamisole (100 mM diluted in IMage-iT FX Signal Enhancer medium; ThermoFisher Item no. I36933) on 3% agarose pads on slides and covered with high-performance cover glass (Zeiss, Item no. 474030-9020-000). To prevent contaminating signal from dust and other particles, before use, the high-performance cover glass was placed in a coverslip holder, cleaned with 200-proof ethanol for 30 minutes (ThermoFisher Item no. 04-355-451), rinsed three times with HPLC H_2O shaking for 10 minutes (ThermoFisher Item no. W5-4), then covered with foil and dried on a heat block. EV images were collected with an

Andor Dragonfly microscope and Andor Zyla sCMOS detector using total internal reflection fluorescence (TIRF) microscopy. The TIRF angle of incidence was manually adjusted for each animal to achieve critical angle. All images of released EVs were taken 30 ± 5 minutes after each animal was immobilized on the agar pad; control and experimental strains were always imaged on the same day. Imaris software (Oxford Instruments) was used to quantitate the number of EVs released into the environment from each male tail. EVs were identified using the “Spot” function, setting object size to 0.350 µm in diameter. A quality threshold was set for each dataset, as determined by analysis of negative controls. Hot pixels were manually removed. EVs that contained both PKD-2 and CLHM-1 were identified as GFP and RFP spots with a maximum distance of 0.3 µm; these data are presented as the probability of PKD-2::GFP being found in a CLHM-1::tdT EV.

Brood size and embryonic viability assays

Analysis of brood size and embryonic viability was conducted as described (Kwah and Jaramillo-Lambert, 2023). The brood size for each worm was determined as the number of unhatched embryos plus the number of live progeny. Embryonic viability was calculated as the number of live progeny divided by the total number of progeny, multiplied by 100.

Analysis of male mating behavior

The day before recording male mating behaviors, 3 cm low peptone (0.4g/L) NGM plates were seeded with 2 drops of 2.5 µl freshly cultured OP50. 24 hours later, ten young adult hermaphrodites were picked onto the mating plates and allowed to settle on the bacterial lawns before introducing a single age-synchronized young male worm. The male was recorded for 15 minutes with an AmScope (MU1000) camera and Amlite software. Male behaviors, including ventral touch time (min), vulva touch time (min), and the number of turns were determined through frame by frame analysis of the recordings.

Statistical Analysis

All statistical analyses and graphing were performed using GraphPad Prism version 10.1.2. Dataset normality was determined using the Anderson-Darling normality test. Depending on normality, either the Student's *t* test or Mann-Whitney U test was used when comparing two datasets and one-way ANOVA or Kruskal-Wallis test with multiple comparisons when comparing three or more datasets; a bionomial test was used to analyze binary data (*p< 0.05, **p< 0.01, ***p< 0.001, ****p<0.0001). Statistical details for individual experiments are specified in the figure legends.

Acknowledgments

We thank the *Caenorhabditis* Genetics Center, which is supported by the NIH-ORIP (P40 OD010440), for strains. The authors also thank the University of Delaware BioImaging facility for their support, which was essential for this work. Microscopy access was supported by National Institutes of Health NIGMS P20 GM103446, NIH-NIGMS P20 GM139760, and the State of Delaware; microscopy equipment was acquired with NIGMS S10 OD030321.

Competing interests

No competing interests declared

Funding

This work was supported by the National Institutes of Health NIGMS T32 GM133395 (to M.E. as part of the Chemistry Biology Interface predoctoral training program), NIGMS R01 GM135433 (to J.E.T.), and Common Fund R03 TR004480 (to J.E.T.).

Author Contributions

Conceptualization, M.W.E., A.E.S., and J.E.T.; Methodology, M.W.E., A.E.S., T.K., and J.E.T.; Investigation, M.W.E., A.E.S., K.D.P., N.S.P., and T.K.; Formal Analysis, M.W.E., A.E.S., K.D.P., N.S.P., T.K, and J.E.T. ; Writing – original draft, M.W.E., A.E.S.,

and J.E.T; Writing – review and editing, M.W.E., A.E.S., K.D.P., N.S.P., T.K, and J.E.T. ; Visualization, M.W.E. and J.E.T.; Supervision, J.E.T.; Funding Acquisition, M.W.E., and J.E.T.

Data Availability

Original data have been deposited at Mendeley Data and will be available as of the date of publication. Individual image files as well as any additional information required to reanalyze the data are available from the corresponding author upon request.

References

Arribere, J. A., Bell, R. T., Fu, B. X. H., Artiles, K. L., Hartman, P. S. and Fire, A. Z. (2014). Efficient marker-free recovery of custom genetic modifications with CRISPR/Cas9 in Caenorhabditis elegans. *Genetics* **198**, 837–846.

Bache, K. G., Raiborg, C., Mehlum, A. and Stenmark, H. (2003). STAM and Hrs are subunits of a multivalent ubiquitin-binding complex on early endosomes. *J. Biol. Chem.* **278**, 12513–12521.

Bae, Y. K., Lyman-Gingerich, J., Barr, M. M. and Knobel, K. M. (2008). Identification of genes involved in the ciliary trafficking of C. elegans PKD-2. *Dev. Dyn.* **237**, 2021–2029.

Bae, Y. K., Kim, E., L'Hernault, S. W. and Barr, M. M. (2009). The CIL-1 PI 5-Phosphatase Localizes TRP Polycystins to Cilia and Activates Sperm in C. elegans. *Curr. Biol.* **19**, 1599–1607.

Balla, T. (2013). Phosphoinositides: tiny lipids with giant impact on cell regulation. *Physiol. Rev.* **93**, 1019–1137.

Barr, M. M. and Sternberg, P. W. (1999). A polycystic kidney-disease gene homologue required for male mating behaviour in C. elegans. *Nature* **401**, 386–389.

Bielas, S. L., Silhavy, J. L., Brancati, F., Kisseleva, M. V, Al-Gazali, L., Sztriha, L., Bayoumi, R. A., Zaki, M. S., Abdel-Aleem, A., Rosti, R. O., et al. (2009). Mutations in INPP5E, encoding inositol polyphosphate-5-phosphatase E, link phosphatidyl inositol signaling to the ciliopathies. *Nat. Genet.* **41**, 1032–1036.

Cao, M., Ning, J., Hernandez-Lara, C. I., Belzile, O., Wang, Q., Dutcher, S. K., Liu, Y. and Snell, W. J. (2015). Uni-directional ciliary membrane protein trafficking by a cytoplasmic retrograde IFT motor and ciliary ectosome shedding. *Elife* **4**,.

Chávez, M., Ena, S., Van Sande, J., de Kerchove d'Exaerde, A., Schurmans, S. and Schiffmann, S. N. (2015). Modulation of Ciliary Phosphoinositide Content Regulates Trafficking and Sonic Hedgehog Signaling Output. *Dev. Cell* **34**, 338–350.

Clement, C. A., Ajbro, K. D., Koefoed, K., Vestergaard, M. L., Veland, I. R., Henriques de Jesus, M. P. R., Pedersen, L. B., Benmerah, A., Andersen, C. Y., Larsen, L. A., et al. (2013). TGF-β signaling is associated with endocytosis at the pocket region of the primary cilium. *Cell Rep.* **3**, 1806–1814.

Clupper, M., Gill, R., Elsayyid, M., Touroutine, D., Caplan, J. L. and Tanis, J. E. (2022). Kinesin-2 motors differentially impact biogenesis of extracellular vesicle subpopulations shed from sensory cilia. *iScience* **25**, 105262.

Conduit, S. E. and Vanhaesebroeck, B. (2020). Phosphoinositide lipids in primary cilia biology. *Biochem. J.* **477**, 3541–3565.

Conduit, S. E., Dyson, J. M. and Mitchell, C. A. (2012). Inositol polyphosphate 5-phosphatases; new players in the regulation of cilia and ciliopathies. *FEBS Lett.* **586**, 2846–2857.

De Craene, J.-O., Bertazzi, D. L., Bär, S. and Friant, S. (2017). Phosphoinositides, Major Actors in Membrane Trafficking and Lipid Signaling Pathways. *Int. J. Mol. Sci.* **18**,.

DiTirro, D., Philbrook, A., Rubino, K. and Sengupta, P. (2019). The Caenorhabditis elegans Tubby homolog dynamically modulates olfactory cilia membrane morphogenesis and phospholipid composition. *Elife* **8**,.

Frøkjær-Jensen, C., Davis, M. W., Ailion, M. and Jorgensen, E. M. (2012). Improved Mos1-mediated transgenesis in C. elegans. *Nat. Methods* **9**, 117–118.

Garcia-Gonzalo, F. R., Phua, S. C., Roberson, E. C., Garcia, G. 3rd, Abedin, M., Schurmans, S., Inoue, T. and Reiter, J. F. (2015). Phosphoinositides Regulate Ciliary Protein Trafficking to Modulate Hedgehog Signaling. *Dev. Cell* **34**, 400–409.

Hodgkin, J., Horvitz, H. R. and Brenner, S. (1979). Nondisjunction Mutants of the Nematode CAENORHABDITIS ELEGANS. *Genetics* **91**, 67.

Honda, A., Nogami, M., Yokozeki, T., Yamazaki, M., Nakamura, H., Watanabe, H., Kawamoto, K., Nakayama, K., Morris, A. J., Frohman, M. A., et al. (1999). Phosphatidylinositol 4-phosphate 5-kinase alpha is a downstream effector of the

small G protein ARF6 in membrane ruffle formation. *Cell* **99**, 521–532.

Hu, J., Wittekind, S. G. and Barr, M. M. (2007). STAM and Hrs Down-Regulate Ciliary TRP Receptors. *Mol. Biol. Cell* **18**, 3277–3289.

Jacoby, M., Cox, J. J., Gayral, S., Hampshire, D. J., Ayub, M., Blockmans, M., Pernot, E., Kisseleva, M. V, Compère, P., Schiffmann, S. N., et al. (2009). INPP5E mutations cause primary cilium signaling defects, ciliary instability and ciliopathies in human and mouse. *Nat. Genet.* **41**, 1027–1031.

Jensen, V. L., Li, C., Bowie, R. V, Clarke, L., Mohan, S., Blacque, O. E. and Leroux, M. R. (2015). Formation of the transition zone by Mks5/Rpgrip1L establishes a ciliary zone of exclusion (CIZE) that compartmentalises ciliary signalling proteins and controls PIP 2 ciliary abundance . *EMBO J.* **34**, 2537–2556.

Kaplan, O. I., Doroquez, D. B., Cevik, S., Bowie, R. V., Clarke, L., Sanders, A. A. W. M., Kida, K., Rappoport, J. Z., Sengupta, P. and Blacque, O. E. (2012). Endocytosis genes facilitate protein and membrane transport in C. elegans sensory cilia. *Curr. Biol.* **22**, 451–460.

Katan, M. and Cockcroft, S. (2020). Phosphatidylinositol(4,5)bisphosphate: diverse functions at the plasma membrane. *Essays Biochem.* **64**, 513–531.

Kelly, W. G., Xu, S., Montgomery, M. K. and Fire, A. (1997). Distinct requirements for somatic and germline expression of a generally expressed Caernorhabditis elegans gene. *Genetics* **146**, 227–238.

Kwah, J. K. and Jaramillo-Lambert, A. (2023). Measuring Embryonic Viability and Brood Size in Caenorhabditis elegans. *J. Vis. Exp.*

Lange, K. I., Tsiropoulou, S., Kucharska, K. and Blacque, O. E. (2021). Interpreting the pathogenicity of joubert syndrome missense variants in caenorhabditis elegans. *DMM Dis. Model. Mech.* **14**,.

Larsch, J., Flavell, S. W., Liu, Q., Gordus, A., Albrecht, D. R. and Bargmann, C. I. (2015). A Circuit for Gradient Climbing in C. elegans Chemotaxis. *Cell Rep.* **12**, 1748–1760.

Li, B., Antonyak, M. A., Zhang, J. and Cerione, R. A. (2012). RhoA triggers a specific signaling pathway that generates transforming microvesicles in cancer cells. *Oncogene* **31**, 4740–4749.

Lloyd, T. E., Atkinson, R., Wu, M. N., Zhou, Y., Pennetta, G. and Bellen, H. J. (2002). Hrs regulates endosome membrane invagination and tyrosine kinase receptor signaling in Drosophila. *Cell* **108**, 261–269.

Lobo, T., Haasnoot, G. H., Nawrocka, A., Bruggeman, C. W., Razzauti, A., Peterman, E. J. G. and Laurent, P. (2025). Sensory stimuli and cilium trafficking defects trigger the release of ciliary extracellular vesicles from multiple ciliary locations. *bioRxiv* 2025.06.06.658075.

Loijens, J. C. and Anderson, R. A. (1996). Type I phosphatidylinositol-4-phosphate 5-kinases are distinct members of this novel lipid kinase family. *J. Biol. Chem.* **271**, 32937–32943.

Luo, N., West, C. C., Murga-Zamalloa, C. A., Sun, L., Anderson, R. M., Wells, C. D., Weinreb, R. N., Travers, J. B., Khanna, H. and Sun, Y. (2012). OCRL localizes to the primary cilium: a new role for cilia in Lowe syndrome. *Hum. Mol. Genet.* **21**, 3333–3344.

Luxmi, R. and King, S. M. (2022). Cilia-derived vesicles: An ancient route for intercellular communication. *Semin. Cell Dev. Biol.* **129**, 82–92.

Luxmi, R., Kumar, D., Mains, R. E., King, S. M. and Eipper, B. A. (2019). Cilia-based peptidergic signaling. *PLoS Biol.* **17**, e3000566.

Maguire, J. E., Silva, M., Nguyen, K. C. Q., Hellen, E., Kern, A. D., Hall, D. H. and Barr, M. M. (2015). Myristoylated CIL-7 regulates ciliary extracellular vesicle biogenesis. *Mol. Biol. Cell* **26**, 2823–2832.

Mill, P., Christensen, S. T. and Pedersen, L. B. (2023). Primary cilia as dynamic and diverse signalling hubs in development and disease. *Nat. Rev. Genet.* **24**, 421–441.

Mizuno, E., Kawahata, K., Kato, M., Kitamura, N. and Komada, M. (2003). STAM proteins bind ubiquitinated proteins on the early endosome via the VHS domain

and ubiquitin-interacting motif. *Mol. Biol. Cell* **14**, 3675–3689.

Molla-Herman, A., Ghossoub, R., Blisnick, T., Meunier, A., Serres, C., Silbermann, F., Emmerson, C., Romeo, K., Bourdoncle, P., Schmitt, A., et al. (2010). The ciliary pocket: an endocytic membrane domain at the base of primary and motile cilia. *J. Cell Sci.* **123**, 1785–1795.

Mukhopadhyay, S., Wen, X., Chih, B., Nelson, C. D., Lane, W. S., Scales, S. J. and Jackson, P. K. (2010). TULP3 bridges the IFT-A complex and membrane phosphoinositides to promote trafficking of G protein-coupled receptors into primary cilia. *Genes Dev.* **24**, 2180–2193.

Mukhopadhyay, S., Wen, X., Ratti, N., Loktev, A., Rangell, L., Scales, S. J. and Jackson, P. K. (2013). The ciliary G-protein-coupled receptor Gpr161 negatively regulates the Sonic hedgehog pathway via cAMP signaling. *Cell* **152**, 210–223.

Muralidharan-Chari, V., Clancy, J., Plou, C., Romao, M., Chavrier, P., Raposo, G. and D'Souza-Schorey, C. (2009). ARF6-Regulated Shedding of Tumor Cell-Derived Plasma Membrane Microvesicles. *Curr. Biol.* **19**, 1875–1885.

Nager, A. R., Goldstein, J. S., Herranz-Pérez, V., Portran, D., Ye, F., Garcia-Verdugo, J. M. and Nachury, M. V. (2017). An Actin Network Dispatches Ciliary GPCRs into Extracellular Vesicles to Modulate Signaling. *Cell* **168**, 252-263.e14.

Nikonorova, I. A., Wang, J., Cope, A. L., Tilton, P. E., Power, K. M., Walsh, J. D., Akella, J. S., Krauchunas, A. R., Shah, P. and Barr, M. M. (2022). Isolation, profiling, and tracking of extracellular vesicle cargo in Caenorhabditis elegans. *Curr. Biol.* **32**, 1924-1936.e6.

O'Hagan, R., Silva, M., Nguyen, K. C. Q., Zhang, W., Bellotti, S., Ramadan, Y. H., Hall, D. H. and Barr, M. M. (2017). Glutamylation Regulates Transport, Specializes Function, and Sculpts the Structure of Cilia. *Curr. Biol.* **27**, 3430-3441.e6.

Ojeda Naharros, I. and Nachury, M. V (2022). Shedding of ciliary vesicles at a glance. *J. Cell Sci.* **135**,.

Park, K. and Leroux, M. R. (2022). Composition, organization and mechanisms of the

transition zone, a gate for the cilium. *EMBO Rep.* **23**, e55420.

Peden, E. M. and Barr, M. M. (2005). The KLP-6 Kinesin Is Required for Male Mating Behaviors and Polycystin Localization in Caenorhabditis elegans. *Curr. Biol.* **15**, 394–404.

Pedersen, L. B., Mogensen, J. B. and Christensen, S. T. (2016). Endocytic Control of Cellular Signaling at the Primary Cilium. *Trends Biochem. Sci.* **41**, 784–797.

Phua, S. C., Chiba, S., Suzuki, M., Su, E., Roberson, E. C., Pusapati, G. V., Setou, M., Rohatgi, R., Reiter, J. F., Ikegami, K., et al. (2017). Dynamic Remodeling of Membrane Composition Drives Cell Cycle through Primary Cilia Excision. *Cell* **168**, 264-279.e15.

Posor, Y., Eichhorn-Grünig, M. and Haucke, V. (2015). Phosphoinositides in endocytosis. *Biochim. Biophys. Acta* **1851**, 794–804.

Raiborg, C., Bache, K. G., Gillooly, D. J., Madshus, I. H., Stang, E. and Stenmark, H. (2002). Hrs sorts ubiquitinated proteins into clathrin-coated microdomains of early endosomes. *Nat. Cell Biol.* **4**, 394–398.

Razzauti, A. and Laurent, P. (2021). Ectocytosis prevents accumulation of ciliary cargo in C. elegans sensory neurons. *Elife* **10**,.

Rbaibi, Y., Cui, S., Mo, D., Carattino, M., Rohatgi, R., Satlin, L. M., Szalinski, C. M., Swanhart, L. M., Fölsch, H., Hukriede, N. A., et al. (2012). OCRL1 modulates cilia length in renal epithelial cells. *Traffic* **13**, 1295–1305.

Scheidel, N., Kennedy, J. and Blacque, O. E. (2018). Endosome maturation factors Rabenosyn-5/VPS45 and caveolin-1 regulate ciliary membrane and polycystin-2 homeostasis. *EMBO J.* **37**,.

Silva, M., Morsci, N., Nguyen, K. C. Q., Rizvi, A., Rongo, C., Hall, D. H. and Barr, M. M. (2017). Cell-Specific α-Tubulin Isotype Regulates Ciliary Microtubule Ultrastructure, Intraflagellar Transport, and Extracellular Vesicle Biology. *Curr. Biol.* **27**, 968–980.

Srinivasan, J., Kaplan, F., Ajredini, R., Zachariah, C., Alborn, H. T., Teal, P. E. A., Malik, R. U., Edison, A. S., Sternberg, P. W. and Schroeder, F. C. (2008). A blend of small molecules regulates both mating and development in Caenorhabditis elegans. *Nature* **454**, 1115–1118.

Stauffer, T. P., Ahn, S. and Meyer, T. (1998). Receptor-induced transient reduction in plasma membrane PtdIns(4,5)P2 concentration monitored in living cells. *Curr. Biol.* **8**, 343–346.

Stilling, S., Kalliakoudas, T., Benninghoven-Frey, H., Inoue, T. and Falkenburger, B. H. (2022). PIP(2) determines length and stability of primary cilia by balancing membrane turnovers. *Commun. Biol.* **5**, 93.

Tanis, J. E., Ma, Z., Krajacic, P., He, L., Foskett, J. K. and Lamitina, T. (2013). CLHM-1 is a Functionally Conserved and Conditionally Toxic Ca2+-Permeable Ion Channel in Caenorhabditis elegans. *J. Neurosci.* **33**, 12275–12286.

Touroutine, D. and Tanis, J. E. (2020). A Rapid, SuperSelective Method for Detection of Single Nucleotide Variants in Caenorhabditis elegans . *Genetics*.

Ukhanov, K., Uytingco, C., Green, W., Zhang, L., Schurmans, S. and Martens, J. R. (2022). INPP5E controls ciliary localization of phospholipids and the odor response in olfactory sensory neurons. *J. Cell Sci.* **135**,.

van Niel, G., D'Angelo, G. and Raposo, G. (2018). Shedding light on the cell biology of extracellular vesicles. *Nat. Rev. Mol. Cell Biol.* **19**, 213–228.

Wang, J., Silva, M., Haas, L. A., Morsci, N. S., Nguyen, K. C. Q., Hall, D. H. and Barr, M. M. (2014). C. elegans Ciliated Sensory Neurons Release Extracellular Vesicles that Function in Animal Communication. *Curr. Biol.* **24**, 519–525.

Wang, J., Kaletsky, R., Silva, M., Williams, A., Haas, L. A., Androwski, R. J., Landis, J. N., Patrick, C., Rashid, A., Santiago-Martinez, D., et al. (2015). Cell-Specific Transcriptional Profiling of Ciliated Sensory Neurons Reveals Regulators of Behavior and Extracellular Vesicle Biogenesis. *Curr. Biol.* **25**, 3232–3238.

Wang, J., Nikonorova, I. A., Gu, A., Sternberg, P. W. and Barr, M. M. (2020).

Release and targeting of polycystin-2-carrying ciliary extracellular vesicles. *Curr. Biol.* **30**, R755–R756.

Wang, J., Nikonorova, I. A., Silva, M., Walsh, J. D., Tilton, P. E., Gu, A., Akella, J. S. and Barr, M. M. (2021). Sensory cilia act as a specialized venue for regulated extracellular vesicle biogenesis and signaling. *Curr. Biol.*

Wang, J., Saul, J., Nikonorova, I. A., Cruz, C. N., Power, K. M., Nguyen, K. C., Hall, D. H. and Barr, M. M. (2024a). Ciliary intrinsic mechanisms regulate dynamic ciliary extracellular vesicle release from sensory neurons. *Curr. Biol.* **34**, 2756-2763.e2.

Wang, J., Barr, M. M. and Wehman, A. M. (2024b). Extracellular vesicles. *Genetics* **227**,.

Weernink, P. A. O., Meletiadis, K., Hommeltenberg, S., Hinz, M., Ishihara, H., Schmidt, M. and Jakobs, K. H. (2004). Activation of type I phosphatidylinositol 4-phosphate 5-kinase isoforms by the Rho GTPases, RhoA, Rac1, and Cdc42. *J. Biol. Chem.* **279**, 7840–7849.

Weinkove, D., Bastiani, M., Chessa, T. A. M., Joshi, D., Hauth, L., Cooke, F. T., Divecha, N. and Schuske, K. (2008). Overexpression of PPK-1, the Caenorhabditis elegans Type I PIP kinase, inhibits growth cone collapse in the developing nervous system and causes axonal degeneration in adults. *Dev. Biol.* **313**, 384–397.

Welsh, J. A., Goberdhan, D. C. I., O'Driscoll, L., Buzas, E. I., Blenkiron, C., Bussolati, B., Cai, H., Di Vizio, D., Driedonks, T. A. P., Erdbrügger, U., et al. (2024). Minimal information for studies of extracellular vesicles (MISEV2023): From basic to advanced approaches. *J. Extracell. vesicles* **13**, e12404.

Witten, G., DeMott, E., Huang, G., Zelasko, F., de Jesus, B., Mulchand, C., Schuck, L., Pullman, S., Perez, A., Mahableshwarkar, P., et al. (2023). mScarlet and split fluorophore mScarlet resources for plasmid-based CRISPR/Cas9 knock-in in C. elegans. *microPublication Biol.* **2023**,.

Wood, C. R., Huang, K., Diener, D. R. and Rosenbaum, J. L. (2013). The Cilium Secretes Bioactive Ectosomes. *Curr. Biol.* **23**, 906–911.

Zhang, X., Jefferson, A. B., Auethavekiat, V. and Majerus, P. W. (1995). The protein deficient in Lowe syndrome is a phosphatidylinositol-4,5-bisphosphate 5-phosphatase. *Proc. Natl. Acad. Sci. U. S. A.* **92**, 4853–4856.

Figure Legends

Figure 1. PPK-1 and INPP-1 are expressed in *C. elegans* male tail RnB sensory neurons. (A) Schematic of EV shedding from the cilium distal tip and PCMC of the cilium base into the environment from a male tail *C. elegans* RnB sensory neuron. (B) In the control, *him-5* mutant males, the PI(4,5)P_2 sensor mNG::PLCδ1-PH (top) is absent from the RnB cilium proper; MKS-2::mSc (middle) shows the transition zone (TZ). Right, normalized fluorescence intensity of mNG::PLCδ1-PH along n = 28 RnB cilia. Average TZ length, 1.09 +/- 0.06 µm. (C) mNG::PPK-1 (top) and MKS-2::mSc (middle) in a RnB neuron. Normalized mNG::PPK-1 fluorescence intensity (right) shows abundant PPK-1 in the dendrite and ciliary base with significantly less in the cilium proper; n = 29 cilia. (D) INPP-1::mNG (top) localizes to the cilium proper, TZ (MKS-2::mSc; middle), and distal dendrite. INPP-1::mNG fluorescence (right; normalized) is reduced in the ciliary base; n = 23 cilia. In all images (B-D), the cilium distal tip is oriented to the left; cilium proper ([), transition zone (▼), ciliary base ({), and scale, 2 µm are indicated. All data are presented as mean +/- SEM.

Figure 2. PPK-1 and INPP-1 regulate PI(4,5)P_2 abundance in RnB sensory neuron cilia. (A) mNG::PLCδ1-PH (top) and MKS-2::mSc (middle) in wild-type, PPK-1 overexpression, and *inpp-1(gk3262)* loss of function mutant (Δ*inpp-1*) animals. Identical settings used for all images; cilium distal tip is oriented to the left, cilium proper ([), transition zone (▼), ciliary base ({), and scale, 2 µm are indicated. (B) Sum intensity of mNG::PLCδ1-PH in the cilium proper for control (grey), PPK-1 overexpressor (purple), and *inpp-1* mutant (orange) animals. *inpp-1* mutants showed a significant increase in mNG::PLCδ1-PH signal in the cilium proper compared to control; n ≥ 26 cilia; **** $p < 0.0001$. (C) mNG::PLCδ1-PH fluorescence intensity (mean +/- SEM) in control, PPK-1 overexpressor, and *inpp-1* mutant animals; n ≥ 22 cilia. PPK-1 overexpression increases the abundance of PI(4,5)P_2 in the ciliary base (purple asterisk indicates p is at least < 0.05 for all points indicated). Loss of *inpp-1* significantly increases PI(4,5)P_2 in the cilium proper (orange asterisk indicates p is at least < 0.05 for all points indicated). A one-way ANOVA was performed for each individual point on the line scan in C; data points not

denoted with an asterisk are not significant from the control. (D) Diagram showing INPP-1 and PPK-1 localization as well as how these enzymes affect ciliary PI(4,5)P_2 levels in wild type animals.

Figure 3. Both overexpression of and loss of PPK-1 impacts shedding of CLHM-1-containing EVs (A) Schematic depicting higher ciliary base PI(4,5)P_2 in PPK-1 Oex animals. (B-C) Representative images of CLHM-1::tdT (*henSi3*) and PKD-2::GFP (*henSi20*) EVs released from (B) control and (C) PPK-1 Oex animals. EVs are marked with spots (Imaris software) for visualization; original, non-cropped, unmarked images are in Sup. Fig. S4; scale, 10 µm. (D) PKD-2::GFP EV release is not affected by PPK-1 Oex. (E) Release of CLHM-1::tdT EVs decreases in PPK-1 Oex animals. (F) Probability of PKD-2::GFP presence in a CLHM-1::tdT EV is unchanged by PPK-1 Oex. For (D-F), $n \geq 26$. (G) Brood size and (H) embryonic viability is significantly reduced in animals with the mNG::PPK-1 endogenous reporter (yellow) compared to the control (grey); $n \geq 9$. (I) Release of CLHM-1::tdT EVs increases in mNG::PPK-1 animals, which have partial loss of PPK-1 function; $n \geq 26$. All data are presented as mean +/- SEM, Mann-Whitney test, * $p < 0.05$, **** $p < 0.0001$.

Figure 4. PPK-1 overexpression affects the abundance and localization of EV cargos in the RnB neurons (A) CLHM-1::tdT (top) and MKS-2::mNG (middle) localization in cilia of control and PPK-1 Oex animals. Cilium proper oriented to the left, two representative images shown for the PPK-1 Oex (a, b) to show the different phenotypes observed. (B) Mean fluorescence intensity and (C) volume of CLHM-1::tdT in the ciliary base and cilium proper in control (grey) and PPK-1 Oex (purple) animals; $n \geq 41$. (D) PKD-2::GFP (top) and MKS-2::mSc (middle) in control and PPK-1 Oex animals. (E) Quantification of PKD-2::GFP fluorescence intensity shows altered localization in the TZ and ciliary base PPK-1 Oex animals compared to the control; $n \geq 14$, * indicates p is at least < 0.05 for all points indicated. (F) Percent of MKS-2::mSc TZ volume that overlapped with PKD-2::GFP; $n \geq 23$. (G) CLHM-1::tdT (top) and MKS-2::mNG (middle); same images presented below with altered settings (high green - HG)

to show the absence (control, left) versus presence of the mNG::PPK-1 endogenous reporter (right). (H) Mean fluorescence intensity and (I) volume of CLHM-1::tdT in the ciliary base and cilium proper in control (grey) and mNG::PPK-1 animals (yellow), which have partial loss of PPK-1 function; n ≥ 29. In this figure, all images are labeled as cilium distal tip (↓), cilium proper ([), transition zone (▼), ciliary base ({), and scale, 2 µm. Data are represented as mean +/- SEM; Mann-Whitney test, * $p < 0.05$, **** $p<0.0001$.

Figure 5. Loss of INPP-1 increases the release of PKD-2 ectosoms. (A) Schematic showing high $PI(4,5)P_2$ in both the PCMC and cilium proper in the *inpp-1* mutant. (B-C) Representative images of CLHM-1::tdT and PKD-2::GFP EVs shed from (B) control and (C) *inpp-1* mutant male tails; scale, 10 µm. EVs marked with spots (Imaris software) for visualization; see also Sup. Fig. 4. (C,D) Loss of *inpp-1* causes an increase in the number of PKD-2::GFP EVs released into the environment in two different genetic strains analyzed (D, UDE275; E, UDE340), but does not impact (F) CLHM-1::tdT EV shedding or (G) colocalization of the two cargos in EVs; n ≥ 25. Data are represented as mean +/- SEM; Mann-Whitney test, * $p < 0.05$.

Figure 6. INPP-1 regulates localization of PKD-2 in the RnB neurons. (A) PKD-2::GFP (top) and MKS-2::mSc (middle) in cilia of control and *inpp-1* mutant (two representative cilia; a,b) animals. Identical settings used for all images; cilium distal tip (↓) is oriented to the left; cilium proper ([), transition zone (▼), ciliary base ({), and scale, 2 µm, labeled. (B) Percent of *inpp-1* mutant and control RnB neurons that exhibited PKD-2::GFP in the cilium proper 5 minutes (T0) and 45 minutes (T1) after being prepared for imaging; n ≥ 65. There was no difference at the initial time point, but significantly more *inpp-1* mutant cilia lacked PKD-2::GFP at the later time point. (C) Analysis of only the RnBs with PKD-2::GFP present in the cilium at the first time point, also showed that by the 45 minutes, the *inpp-1* mutant had significantly fewer RnB cilia with PKD-2::GFP. (D) Mean fluorescence intensity and (E) volume of PKD-2::GFP in the cilium proper of control and *inpp-1* mutants. Cilia that lacked PKD-2::GFP signal in the

cilium proper detectable by the Imaris surfaces tool at a threshold of 16 were excluded from this analysis, n = 50. (F) Representative images of PKD-2::GFP and MKS-2::mSc in the RnB neurons of control and (G) *inpp-1* mutant male tails; scale, 10 μm. (H) Loss of *inpp-1* caused a significant increase in the number of RnB neurons with PKD-2 backed-up in the dendrites, defined as the percent of neurons with PKD-2::GFP signal extending greater than 5 μm from the transition zone; n ≥ 66. Data are represented as mean +/- SEM. A binomial test was used for B, C, and I; a Mann-Whitney test was used for D,E. * $p < 0.05$, ** $p< 0.01$, **** $p < 0.0001$.

Figure 7. Loss of *inpp-5k* impacts PKD-2 localization in neurons, but not ectosome release. (A-B) Representative images of PKD-2::GFP (*henSi20*) and MKS-2::mSc in the RnB neurons of (A) control and (B) *inpp-5k* mutant male tails; scale, 10 μm. (C) Loss of *inpp-5k* causes backup of PKD-2::GFP in RnB dendrites. Binary data from n ≥ 40 neurons were analyzed with a binomial test, **** $p<0.0001$. (D) INPP-5K::mNG (top) and MKS-2::mSc (middle) in R4B (left) and R6B (right) neurons. In these images, the cilium proper ([), transition zone (▼), ciliary base ({), and scale, 2 μm, are as indicated. (E) Average INPP-5K::mNG fluorescence intensity shows that INPP-5K is present in the ciliary base of R6B (dark green), but absent from R4B (light green); n ≥ 8 for each RnB cilia. (F) mNG::PLCδ1-PH fluorescence intensity (mean +/- SEM) in control (grey) and *inpp-5k* mutant (blue) animals; n ≥ 13 R3B-R5B cilia analyzed. A small increase in $PI(4,5)P_2$ in the PCMC is observed in the *inpp-5k* mutant; * indicates p is at least < 0.05 for all points indicated. (G) Loss of *inpp-5k* does not impact release of PKD-2::GFP EVs (n ≥ 28), (H) CLHM-1::GFP EVs (n ≥ 31), or (I) distribution of CLHM-1::GFP in the RnB dendrites (n ≥ 45 cilia). Data are represented as mean +/- SEM; A binomial test was used for C and I; a Mann-Whitney test was used for F-H, * $p < 0.05$, **** $p < 0.0001$.

Figure 8. An increase in ciliary $PI(4,5)P_2$ does not impact the length of the cilium proper. (A) Representative images of RnB cilia filled out with KLP-6::GFP (top) in control (left), PPK-1 Oex (middle), and *inpp-1* mutant (right) animals. Cilium distal tip (↓)

is to the left; MKS-2::mSc (middle) marks the TZ (▼); scale, 2 μm. (B) Length and (C) diameter of cilia were unchanged in the PPK-1 Oex (purple) and *inpp-1* mutant (orange) compared to the control (grey); n ≥ 45. Data are represented as mean +/- SEM, mixed-effects model (REML). (D) PPK-1 and INPP-1 regulate PI(4,5)P_2 abundance and distribution in the RnB ciliated sensory neurons; PI(4,5)P_2 is normally absent from the cilium proper (left). Overexpression of PPK-1 (middle) increases PI(4,5)P_2 in the PCMC, which leads to a decrease in CLHM-1 abundance and EV shedding, while reduced PPK-1 function causes an increase in CLHM-1 EV release. Loss of *inpp-1* (right) results in accumulation of PI(4,5)P_2 in the cilium proper and an increase in PKD-2 EV shedding. Increasing PI(4,5)P_2 levels did not impact cilium length.

Supplemental Figure S1. Localization of PI(4,5)P_2 regulatory enzymes in the male tail. (A,B) Endogenously tagged (A) mNG::PPK-1 and (B) INPP-1::mNG with the MKS-2::mSc TZ marker in the RnB neurons of the male tail; scale, 10 μm.

Supplemental Figure S2. Quantification of ciliary proteins. (A) Line scan analysis performed to determine distribution of mNG::PLCδ1-PH (Fig. 1B; Fig. 2D; Fig. 7F), mNG::PPK-1 (Fig. 1C), INPP-1::mNG (Fig. 1D), PKD-2::GFP (Fig. 4E), and INPP-5K::mNG (Fig. 7E) and CLHM-1::tdT (Sup. Fig. S5C). (B) Volumetric and fluorescence intensity analyses (Fig. 2B; Fig. 4B,C,F,H,I; Fig. 6D,E; Sup. Fig. S5A,B) and (C) measurements of cilium length (Fig. 6B,C and Sup. Fig. S7A,B) were carried out on 3D reconstructions.

Supplemental Figure S3. CLHM-1::tdT and PKD-2::GFP label EVs released from male tail RnB neurons. (A) CLHM-1::tdTomato and (B) PKD-2::GFP labeled EVs are identified by Imaris spot detection in TIRF images of males that express the CLHM-1::tdT and PKD-2::GFP single copy transgenes, but not *him-5* control animals; n = 9. (C) Representative image of a CLHM-1::tdT-labeled ectosome (top) adjacent to the ciliary base; TZ labeled with MKS-2::mNG (middle). The ectosomes (↓), cilium proper

([), transition zone (▼), ciliary base ({), and scale, 2 µm are labeled in the merge image (bottom). (D) Quantification of the diameter of CLHM-1::tdT EVs inside the worm, adjacent to the ciliary base as in (C) versus the CLHM-1::tdT EVs released into the external environment; n = 12. No difference in size was detected, indicating that the CLHM-1::tdT EVs that bud from the ciliary base are indeed released into the external environment. Data are represented as mean +/- SEM; Mann-Whitney test, **** $p < 0.0001$.

Supplemental Figure S4. Altered abundance of PI(4,5)P_2 regulatory enzymes impacts EV shedding (A-D) Representative images of PKD-2::GFP (*henSi20*) and CLHM-1::tdT (*henSi3*) labeled-EVs released from (A,C) control, (B) PPK-1 Oex, and (D) *inpp-1* mutant male tails; scale, 10 µm. Images in A,B correspond to Fig. 3B,C; images in C,D correspond to Fig 5B,C.

Supplemental Figure S5. Loss of STAM-1 does not affect CLHM-1 ciliary abundance, localization, or EV release. (A) Mean fluorescence intensity and (B) volume of CLHM-1::tdT in the ciliary base in control (grey) and *stam-1(ok406)* mutants (red); n ≥ 14. (C) Normalized CLHM-1::tdT fluorescence intensity shows that loss of *stam-1* does not impact CLHM-1 distribution between the cilium proper and base; n ≥ 14. (D) Release of CLHM-1::tdT EVs and (E) PKD-2::GFP EVs from the *stam-1* mutant is not significantly different from the control; n ≥ 20. Data are represented as mean +/- SEM; Mann-Whitney test, ns = not significant.

Supplemental Figure S6. The INPP-5K::mNG endogenous reporter retains partial function. (A) Brood size and (B) embryonic viability for wild-type control (grey), *inpp-5k(my15)* mutants (blue), and the INPP-5K::mNG (*syb9399*) endogenous reporter (green). Animals expressing INPP-5K::mNG have a significantly greater brood size compared to the *inpp-5k(my15)* mutant, but reduced brood size and embryonic viability compared to the wild type control, suggesting that insertion of the mNG C-terminal tag

results in partial INPP-5K function. Data are presented as mean +/- SEM, one-way ANOVA, ** $p < 0.01$, **** $p < 0.0001$.

Supplemental Figure S7. Altered PI(4,5)P_2 does not impact cilium length (A) Length measurements of RnB3 (marginal opening), RnB4 (ventral opening), and RnB5 (dorsal opening) cilia in *him-5* control males expressing KLP-6::GFP with MKS-2::mSc; the cilia of these RnB neurons do not differ in length, $n \geq 8$. (B) No significant difference in RnB3, RnB4, and RnB5 cilia lengths is observed between control (grey), $n \geq 10$, *inpp-1* mutant (orange), $n \geq 8$, and PPK-1 Oex (purple) animals, $n \geq 10$. Data are represented as mean +/- SEM.

Supplemental Table 1: Loss of *inpp-1* does not impact male mating behavior. Six parameters of male mating behavior were assessed for control animals and *inpp-1* mutants; both strains contain *him-5(e1490)*, which results in male offspring for analysis.

Supplemental Table 2: *C. elegans* strains used in this work

Figure 1

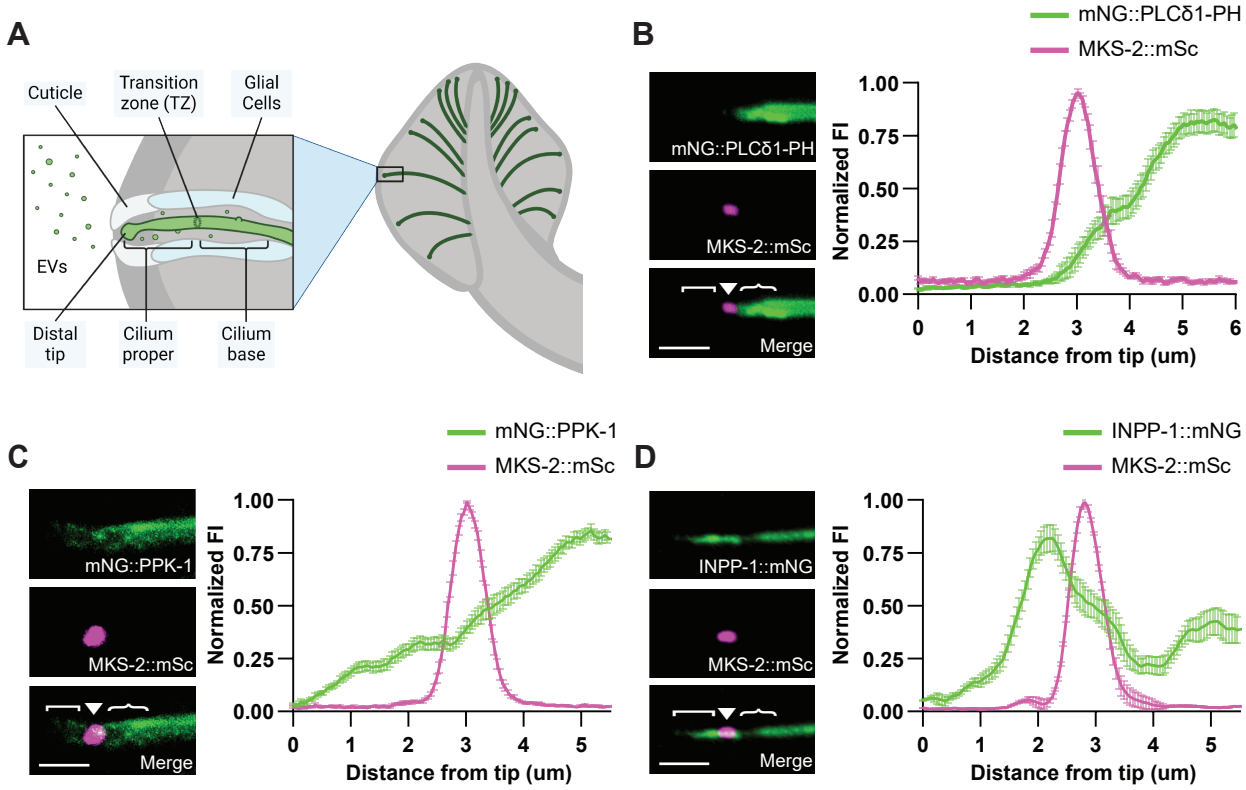
A
Cuticle
Transition zone (TZ)
Glial Cells
EVs
Distal tip
Cilium proper
Cilium base
B
mNG::PLCδ1-PH
MKS-2::mSc
mNG::PLCδ1-PH
MKS-2::mSc
Merge
Normalized FI
Distance from tip (um)
C
mNG::PPK-1
MKS-2::mSc
mNG::PPK-1
MKS-2::mSc
Merge
Normalized FI
Distance from tip (um)
D
INPP-1::mNG
MKS-2::mSc
INPP-1::mNG
MKS-2::mSc
Merge
Normalized FI
Distance from tip (um)

Figure 2

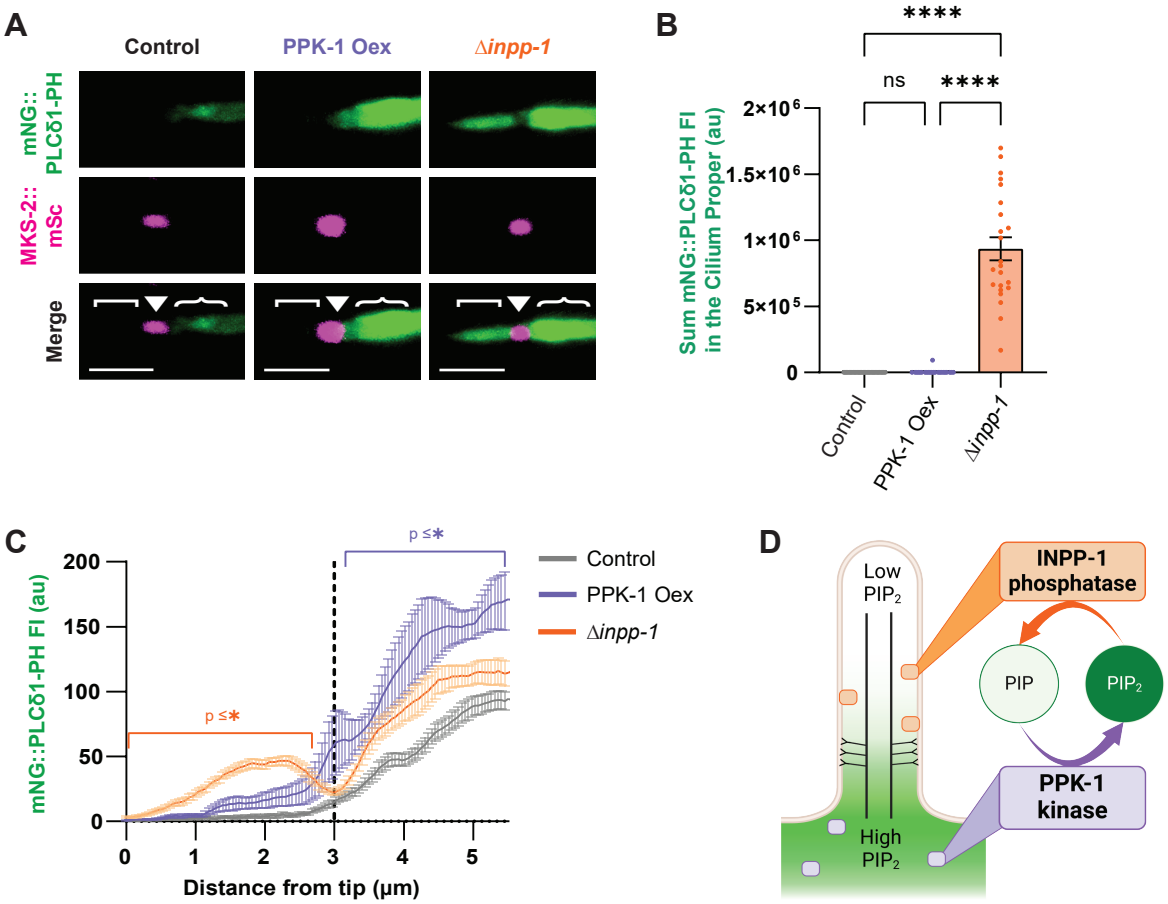
A
Control
PPK-1 Oex
Δinpp-1
mNG::PLCδ1-PH
MKS-2::mSc
Merge
B
****
ns
****
Sum mNG::PLCδ1-PH FI in the Cilium Proper (au)
2×10⁶
1.5×10⁶
1×10⁶
5×10⁵
0
Control
PPK-1 Oex
Δinpp-1
C
mNG::PLCδ1-PH FI (au)
200
150
100
50
0
p ≤*
p ≤*
0
1
2
3
4
5
Distance from tip (μm)
Control
PPK-1 Oex
Δinpp-1
D
Low PIP2
High PIP2
INPP-1 phosphatase
PIP
PIP2
PPK-1 kinase

Figure 3

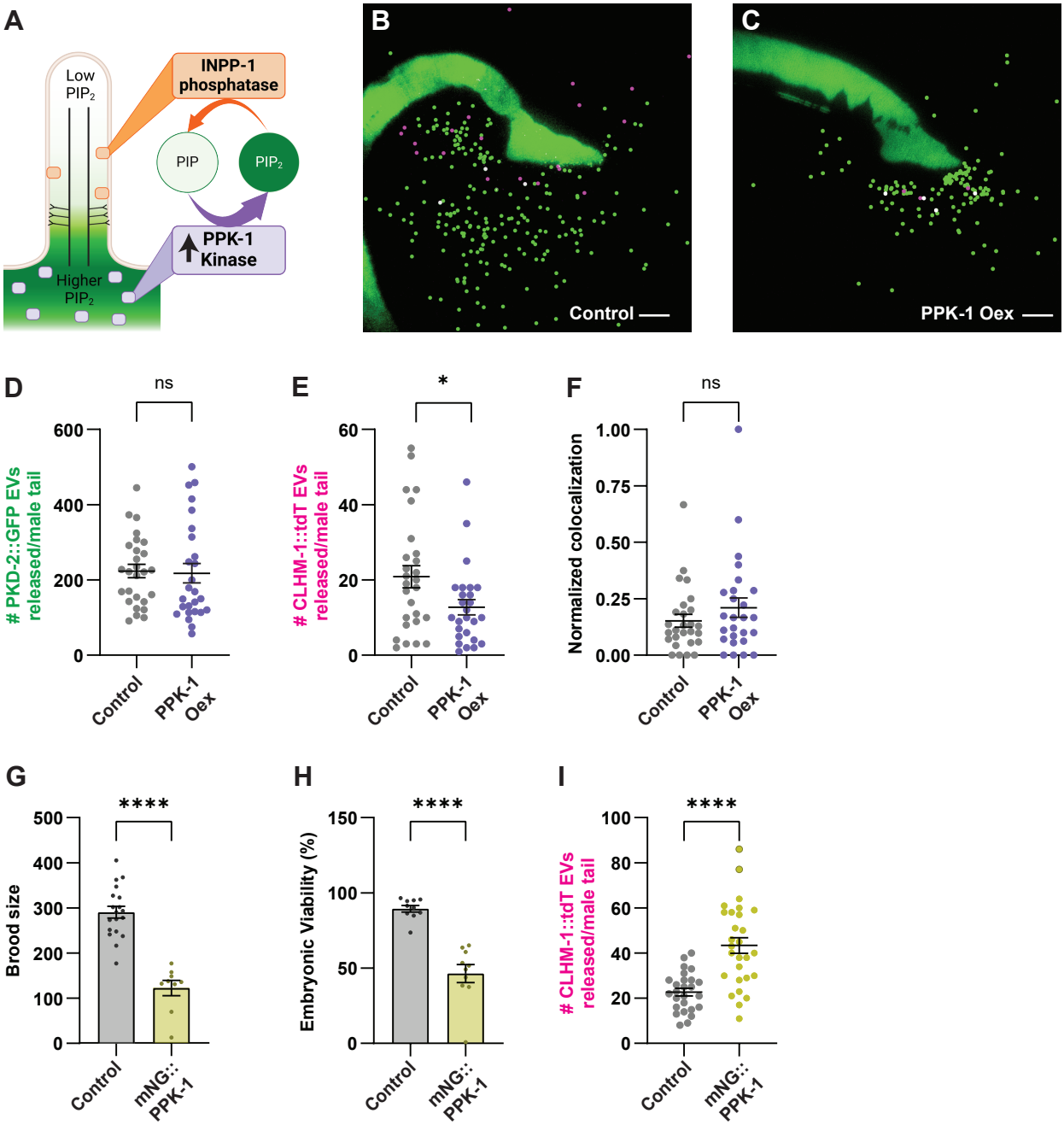
A
Low PIP2
INPP-1 phosphatase
PIP
PIP2
PPK-1 Kinase
Higher PIP2
B
Control
C
PPK-1 Oex
D
ns
PKD-2::GFP EVs released/male tail
600
400
200
0
Control
PPK-1 Oex
E
*
CLHM-1::tdT EVs released/male tail
60
40
20
0
Control
PPK-1 Oex
F
ns
Normalized colocalization
1.00
0.75
0.50
0.25
0.00
Control
PPK-1 Oex
G
****
Brood size
500
400
300
200
100
0
Control
mNG::PPK-1
H
****
Embryonic Viability (%)
150
100
50
0
Control
mNG::PPK-1
I
****
CLHM-1::tdT EVs released/male tail
100
80
60
40
20
0
Control
mNG::PPK-1

Figure 4

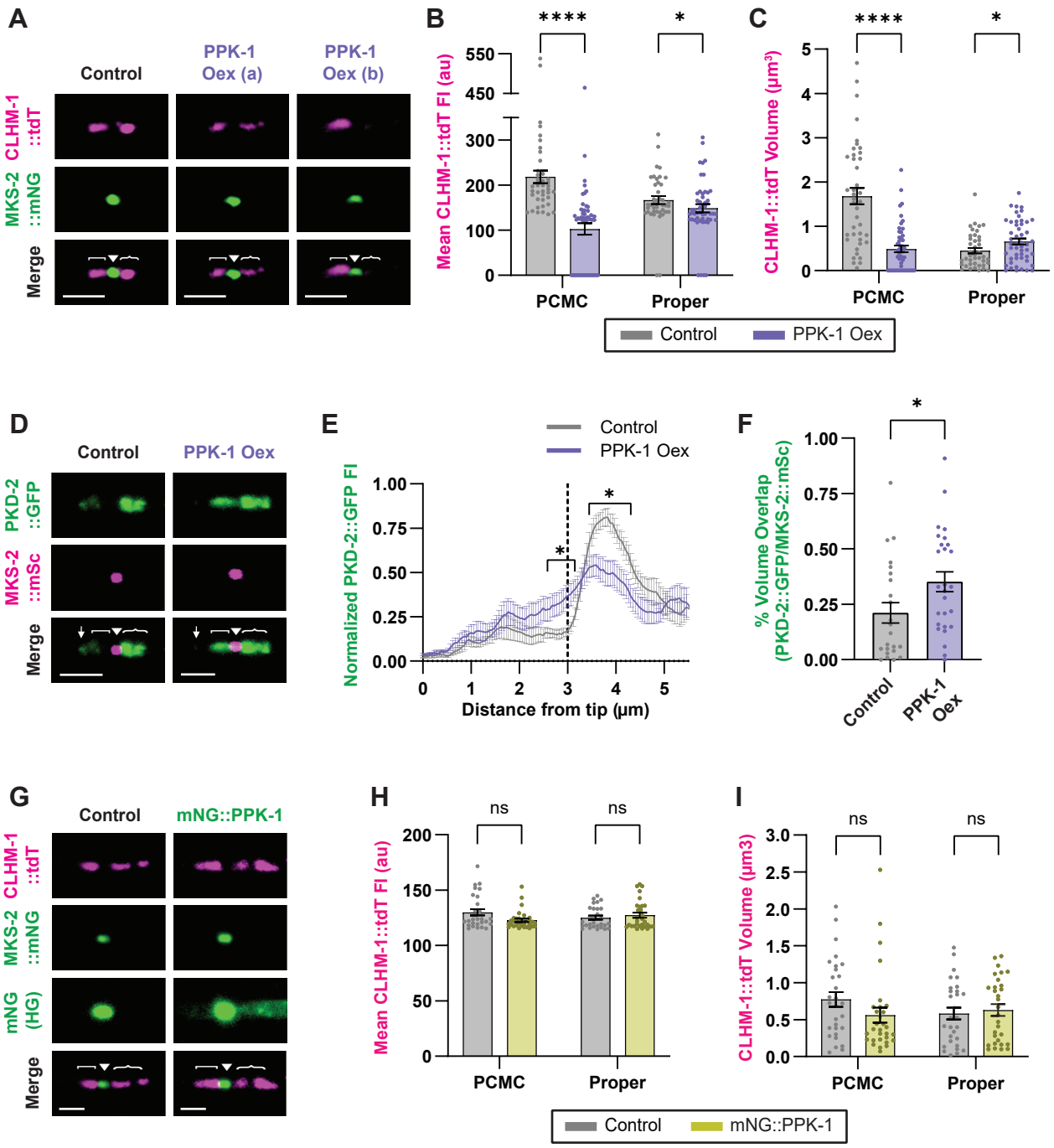
A
Control
PPK-1 Oex (a)
PPK-1 Oex (b)
CLHM-1 ::tdT
MKS-2 ::mNG
Merge
B
Mean CLHM-1::tdT FI (au)
PCMC
Proper
C
CLHM-1::tdT Volume (µm³)
PCMC
Proper
Control
PPK-1 Oex
D
Control
PPK-1 Oex
PKD-2 ::GFP
MKS-2 ::mSc
Merge
E
Control
PPK-1 Oex
Normalized PKD-2::GFP FI
Distance from tip (µm)
F
% Volume Overlap (PKD-2::GFP/MKS-2::mSc)
Control
PPK-1 Oex
G
Control
mNG::PPK-1
CLHM-1 ::tdT
MKS-2 ::mNG
mNG (HG)
Merge
H
Mean CLHM-1::tdT FI (au)
PCMC
Proper
I
CLHM-1::tdT Volume (µm3)
PCMC
Proper
Control
mNG::PPK-1

Figure 5

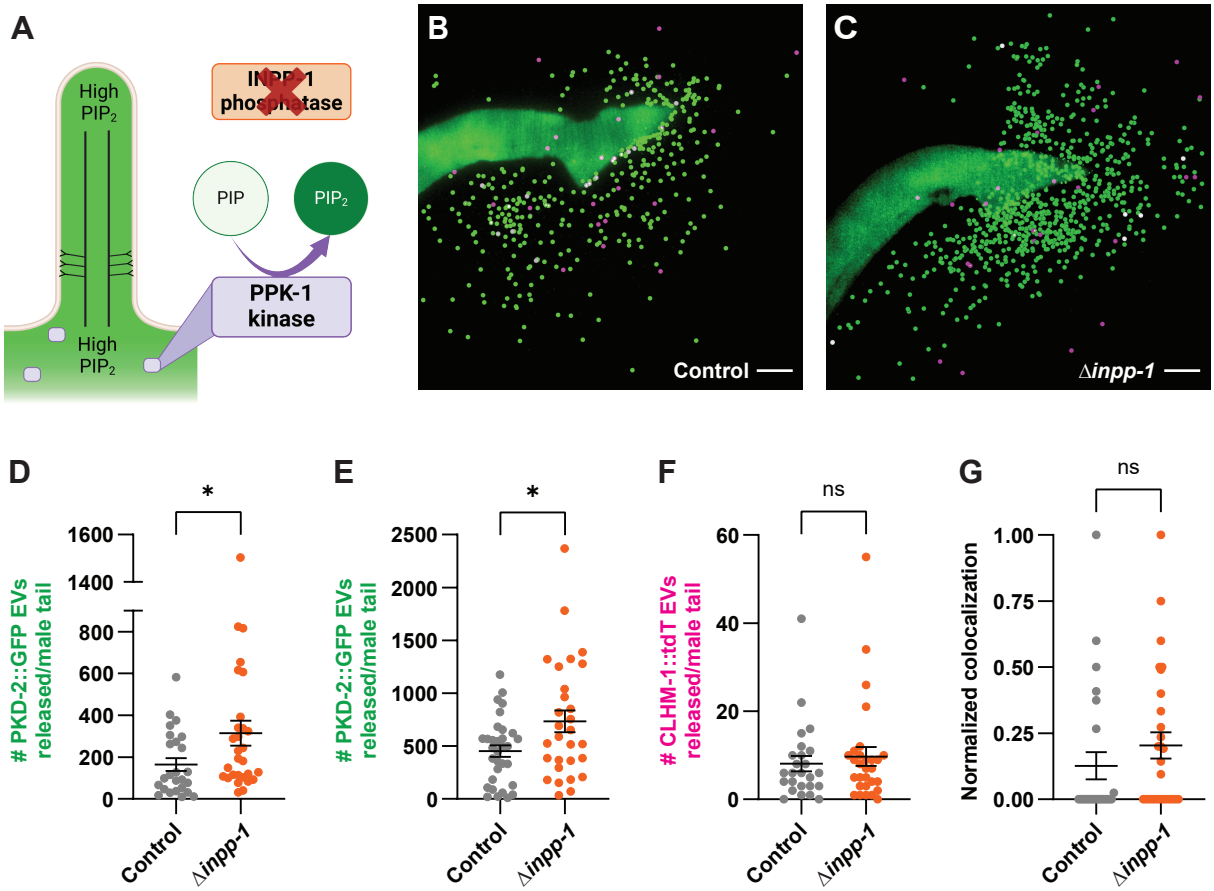
A
High PIP2
INPP-1 phosphatase
PIP
PIP2
PPK-1 kinase
High PIP2
B
Control
C
Δinpp-1
D
PKD-2::GFP EVs released/male tail
1600
1400
800
600
400
200
0
*
Control
Δinpp-1
E
PKD-2::GFP EVs released/male tail
2500
2000
1500
1000
500
0
*
Control
Δinpp-1
F
CLHM-1::tdT EVs released/male tail
60
40
20
0
ns
Control
Δinpp-1
G
Normalized colocalization
1.00
0.75
0.50
0.25
0.00
ns
Control
Δinpp-1

Figure 6

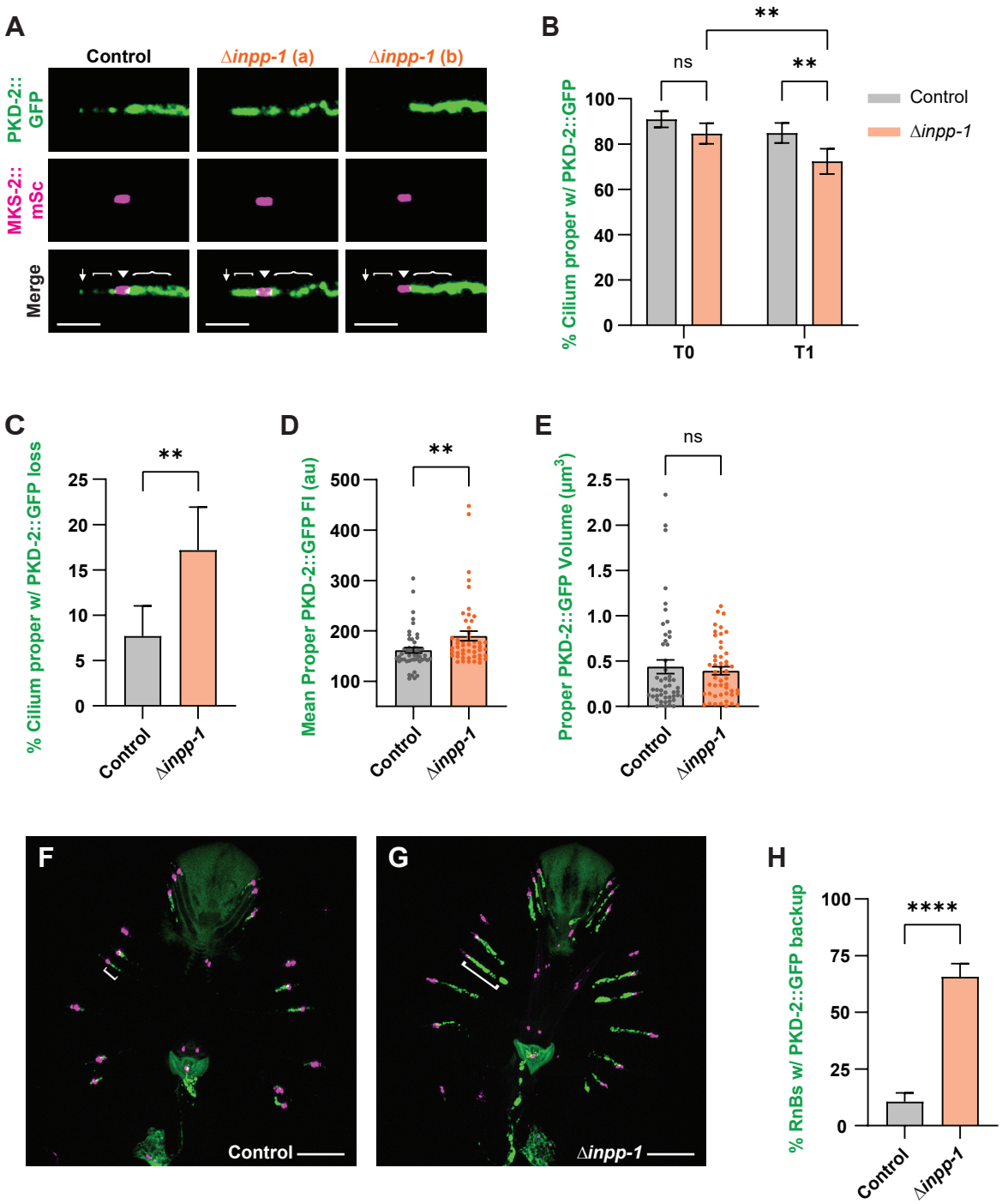
A
Control
Δinpp-1 (a)
Δinpp-1 (b)
PKD-2::GFP
MKS-2::mSc
Merge
B
**
ns
**
% Cilium proper w/ PKD-2::GFP
100
80
60
40
20
0
T0
T1
Control
Δinpp-1
C
**
% Cilium proper w/ PKD-2::GFP loss
25
20
15
10
5
0
Control
Δinpp-1
D
**
Mean Proper PKD-2::GFP FI (au)
500
400
300
200
100
Control
Δinpp-1
E
ns
Proper PKD-2::GFP Volume (μm3)
2.5
2.0
1.5
1.0
0.5
0.0
Control
Δinpp-1
F
Control
G
Δinpp-1
H
****
% RnBs w/ PKD-2::GFP backup
100
75
50
25
0
Control
Δinpp-1

Figure 7

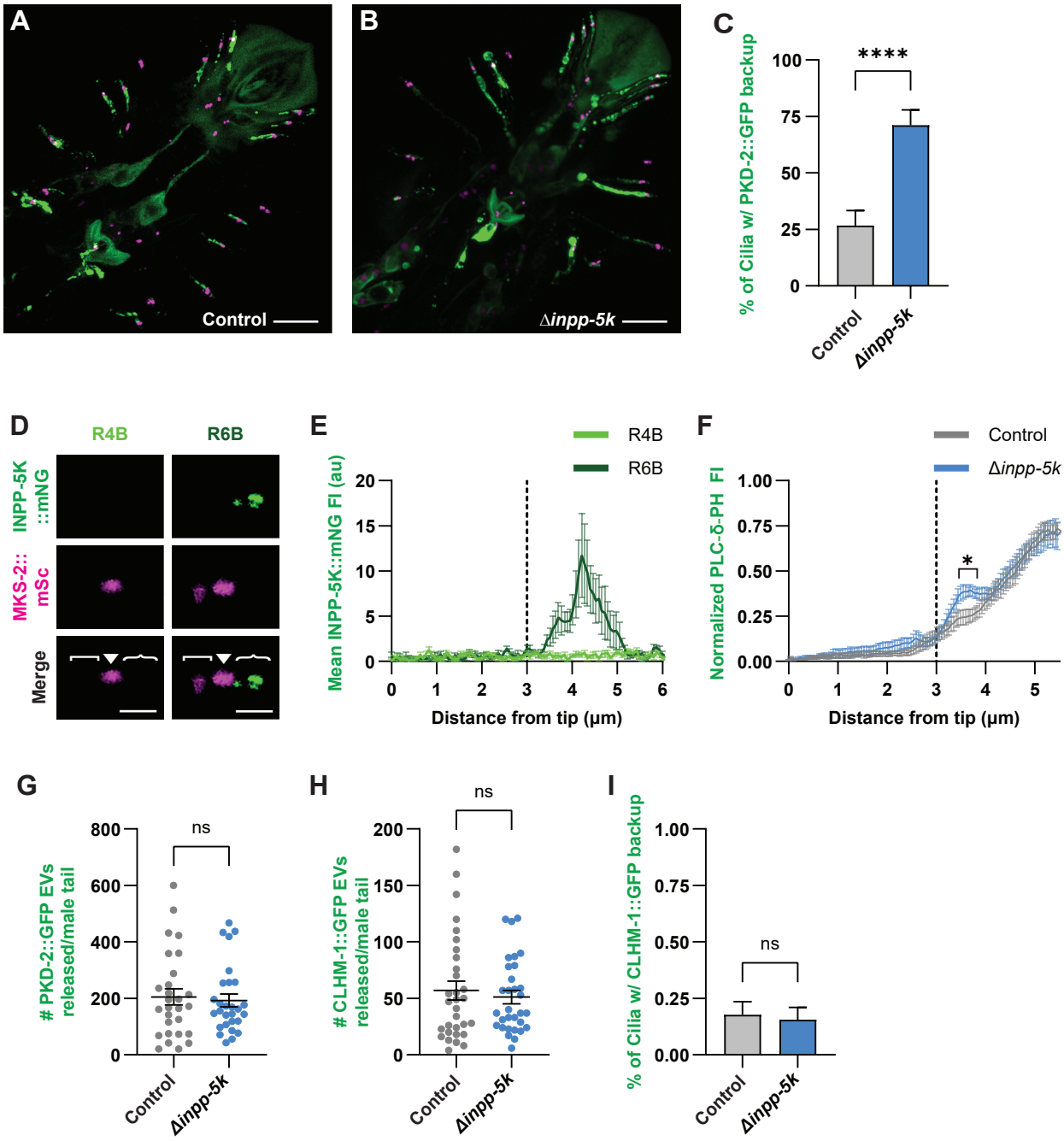
A
Control
B
Δinpp-5k
C
% of Cilia w/ PKD-2::GFP backup
****
Control
Δinpp-5k
D
R4B
R6B
INPP-5K ::mNG
MKS-2:: mSc
Merge
E
R4B
R6B
Mean INPP-5K::mNG FI (au)
Distance from tip (μm)
F
Control
Δinpp-5k
Normalized PLC-δ-PH FI
*
Distance from tip (μm)
G
PKD-2::GFP EVs released/male tail
ns
Control
Δinpp-5k
H
CLHM-1::GFP EVs released/male tail
ns
Control
Δinpp-5k
I
% of Cilia w/ CLHM-1::GFP backup
ns
Control
Δinpp-5k

Figure 8

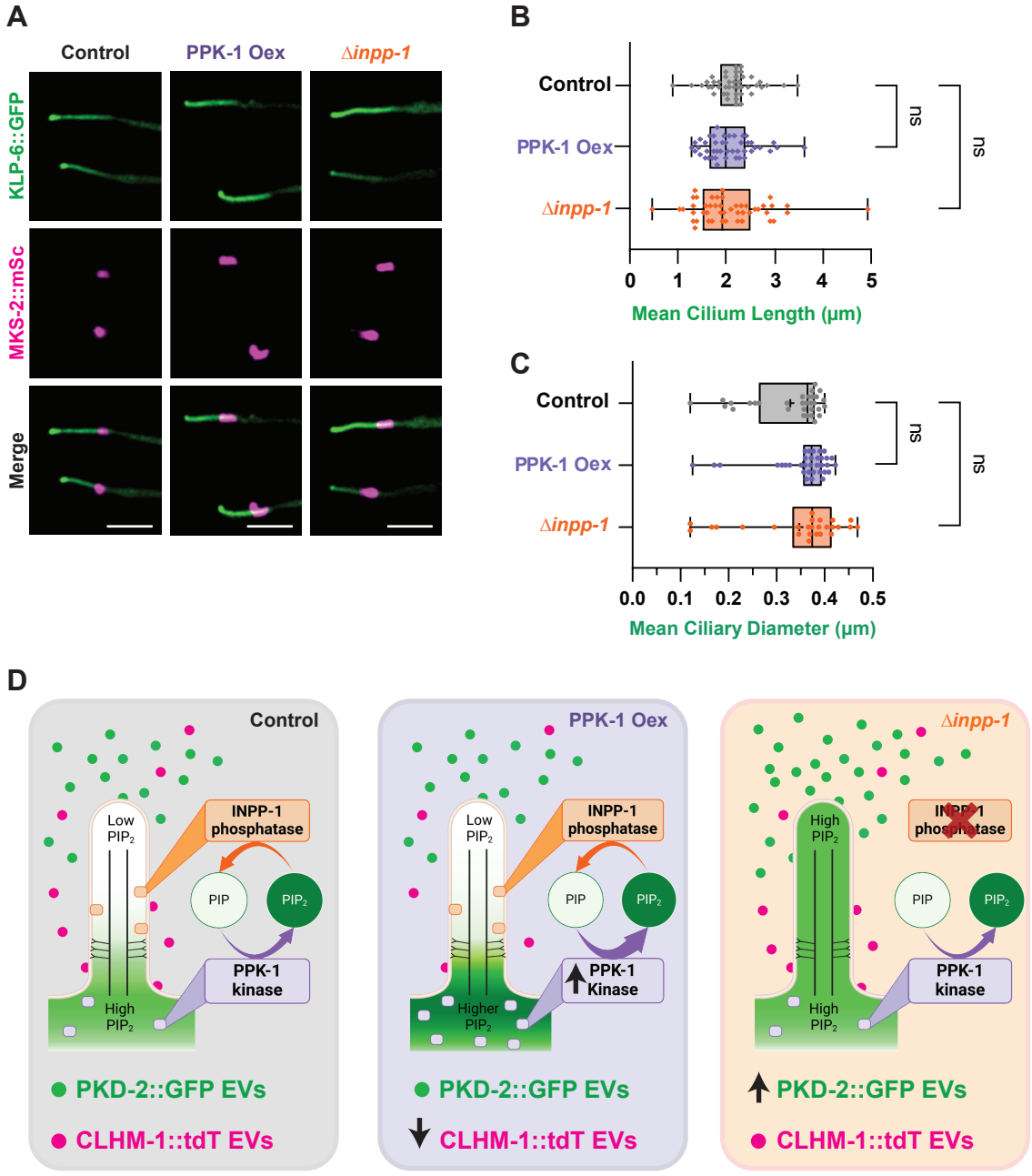
A
Control
PPK-1 Oex
Δinpp-1
KLP-6::GFP
MKS-2::mSc
Merge
B
Control
PPK-1 Oex
Δinpp-1
ns
ns
0
1
2
3
4
5
Mean Cilium Length (μm)
C
Control
PPK-1 Oex
Δinpp-1
ns
ns
0.0
0.1
0.2
0.3
0.4
0.5
Mean Ciliary Diameter (μm)
D
Control
Low PIP2
INPP-1 phosphatase
PIP
PIP2
PPK-1 kinase
High PIP2
PKD-2::GFP EVs
CLHM-1::tdT EVs
PPK-1 Oex
Low PIP2
INPP-1 phosphatase
PIP
PIP2
PPK-1 Kinase
Higher PIP2
PKD-2::GFP EVs
CLHM-1::tdT EVs
Δinpp-1
High PIP2
PIP
PIP2
PPK-1 kinase
High PIP2
PKD-2::GFP EVs
CLHM-1::tdT EVs